Bioorganic Chemistry 130 (2023) 106234

Contents lists available at ScienceDirect

Bioorganic Chemistry

journal homepage: www.elsevier.com/locate/bioorg

Structural optimization of novel Ras modulator for treatment of Colorectal cancer by promoting β-catenin and Ras degradation

Seonghwi Choi [a,1], Hyuntae Kim [a,1], Won-Ji Ryu [b], Kang-Yell Choi [b], Taegun Kim [b], Doona Song [b], Gyoonhee Han [a,b,c,d,*]

[a] Department of Interdisciplinary Program of Integrated OMICS for Biomedical Sciences, Yonsei University, Seoul 03722, Republic of Korea
[b] Department of Biotechnology, Yonsei University, Seoul 03722, Republic of Korea
[c] Department of Pharmacy, College of Pharmacy, Yonsei University, Incheon 21983, Republic of Korea
[d] S2C bio Inc., Songdogwahak-ro, Incheon, 21983, Republic of Korea

ARTICLE INFO

Keywords:
Colorectal cancer
Ras
β-catenin
β-catenin Destruction complex
Axin

ABSTRACT

Ras protein has been considered a fascinating target for anticancer therapy because its malfunction is closely related to cancer. However, Ras has been considered undruggable because of the failure to regulate its malfunction by controlling the Ras activation mechanism. Recently, Lumakras targeting the G12C mutation was approved, and therapeutic interest in Ras for anticancer therapy has been rejuvenated. Here, we present a series of compounds that inhibit Ras via a unique mechanism of action that exploits the relationship between the Wnt/β-catenin pathway and Ras. **KYA1797K (1)** binds to axin to stabilize the β-catenin destruction complex that causes the phosphorylation and subsequent degradation of Ras, similar to canonical β-catenin regulation. Based on the chemical structure of **1**, we performed a structural optimization and identified 3-(2-hydroxyethyl)-5-((6-(4-nitrophenyl)pyridin-2-yl)methylene)thiazolidine-2,4-dione (**13d**) as the most potent compound. **13d** displayed antitumor effects in a colorectal cancer model with enhanced inhibition activity on Ras. The results of this study suggest that the further development of **13d** could contribute to the development of Ras inhibitors with novel mechanisms of action.

1. Introduction

Colorectal cancer (CRC) accounts for a significant proportion of cancer incidence (10 %) and mortality (9 %) of all cancers worldwide. [1] Among the major causes of CRC is Ras, a controller of signal cascades. [2] Abnormal activity of Ras significantly contributes to the malignant progression of CRC along with mutation in APC (Adenomatous Polyposis Coli), a regulator of the Wnt/β-catenin pathway. [3,4].

Ras is a membrane-bound G protein involved in cell growth, survival, and differentiation by transmitting extracellular stimulation to cytoplasmic signal cascades. Ligands such as epidermal growth factors (EGFs) interact with receptor tyrosine kinases (RTKs) to form receptor dimers that attract Grb2 (growth factor receptor-bound protein 2) and Sos (Son of sevenless). [5] The receptor-Grb2-Sos complex recruits and activates Ras. [6] Activated Ras acts on diverse signaling pathways through the "on switch" role of its downstream molecules such as PI3K, Raf, and Ral. [7,8].

Ras activity is tightly regulated by guanine nucleotide exchange factors (GEFs) and GAPs (GTPase activating proteins) between the inactive GDP-bound and the active GTP-bound states. [9] GEFs such as Sos induce conformational changes in Ras such that it has a high affinity for GTP. [10] GTP-bound Ras acquires a higher affinity to its effectors and activates downstream signals unless it is converted to the resting state by GAPs. GAPs accelerate the innate GTPase activity of Ras, which results in the hydrolysis of the bound GTP. [11] Mutations in Ras disrupt the regulatory mechanisms, allowing Ras to stimulate signaling pathways constitutively. [12].

Owing to its major role in tumorigenesis, Ras has attracted tremendous therapeutic interest for decades (Fig. 1). [13] Farnesyltransferase inhibitors (Tipifarnib and Lonafarnib) and phosphodiesterase δ

Abbreviations: APC, Adenomatous polyposis coli; CRC, Colorectal cancer; Ras, Rat sarcoma virus; RGS, Regulator of G protein signaling; TZD, 2,4-dioxothiazolidine (2,4-thiazolidinedione); TOPflash, TCF reporter plasmid.

* Corresponding author.
E-mail address: gyoonhee@yonsei.ac.kr (G. Han).
[1] These authors contributed equally.

https://doi.org/10.1016/j.bioorg.2022.106234
Received 26 August 2022; Received in revised form 25 October 2022; Accepted 29 October 2022
Available online 4 November 2022

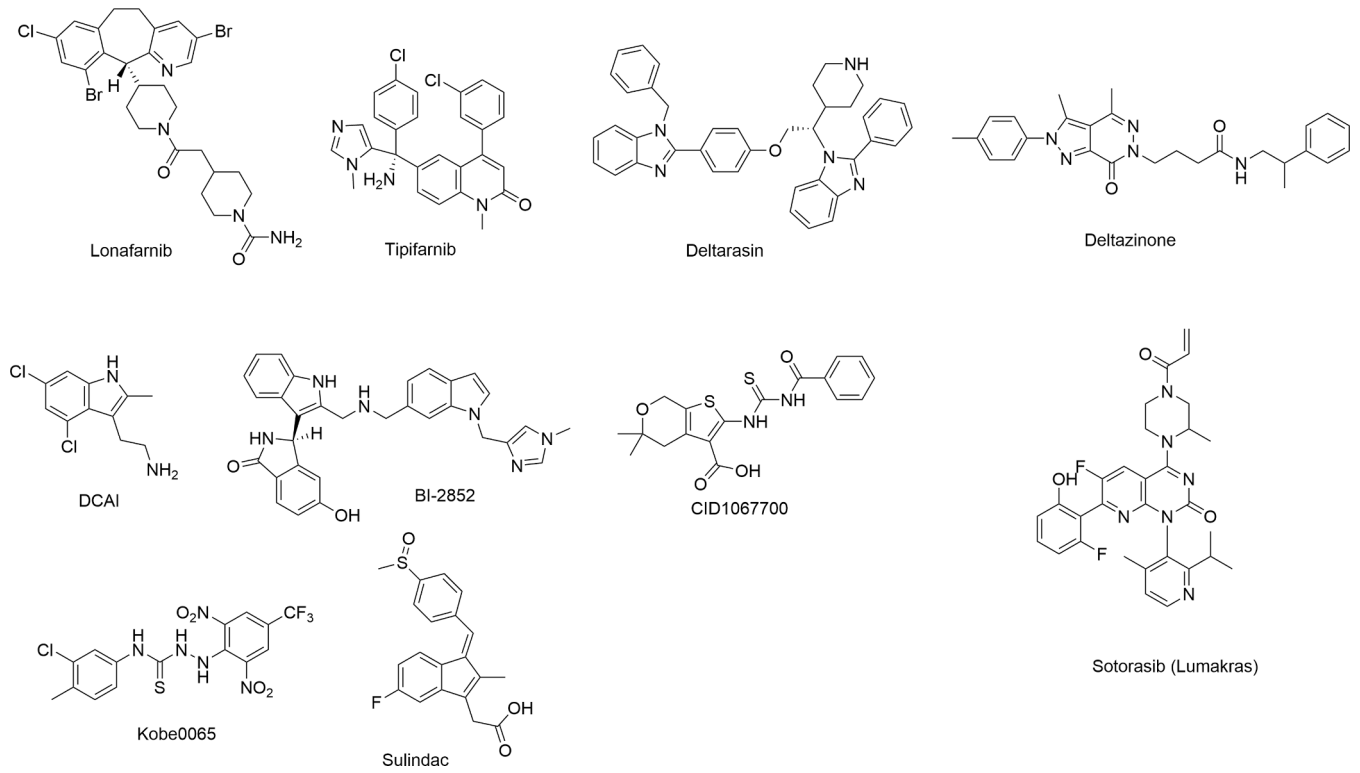

Fig. 1. Structures of Ras inhibitors. Sotorasib (Lumakras), which specifically targets Ras ^{G12C}, was approved for the treatment of non-small cell lung cancer in May 2021.

inhibitors (Deltarasin and Deltazinone) were designed to disrupt the membrane localization of Ras. [14 –18] DCAI and BI-2852 interrupted the Ras-Sos interaction, and CID1067700 competed with GTP to hinder the activation of Ras. [19 –21] Sulindac and Kobe0065 derivatives interrupted the activity of Ras by blocking the interaction between Ras and its downstream effectors. [22,23] However, these inhibitors failed to prove their effectiveness in preclinical or clinical stages because of alternative modifications, high Ras-GTP affinity, or limited specificity and activity. [13] Due to the failure to develop these inhibitors, Ras was considered an undruggable target until the first anti-Ras drug, Lumakras (Sotorasib, AMG510), was approved by the FDA for the treatment of NSCLC in May 2021. [24] Lumakras inhibited Ras^{G12C} by blocking GTP entry through formation of a covalent bond with the cysteine in the mutated Ras. [25] Although Lumakras has demonstrated the possibility of Ras inhibitors, drug resistance is highly likely to develop through off-target mutations, like other targeted therapies. Therefore, approaches to target degradation of Ras protein regardless of mutation, such as PROTAC, are emerging. [26,27] In this study, we suggest the possibility of developing a pan-Ras inhibitor with a unique mechanism of action that promotes the degradation of Ras by harnessing its interactions with the Wnt/β-catenin signaling pathway. [3,28].

In the Wnt/β-catenin canonical pathway, β-catenin is regulated by a protein complex called the destruction complex, which comprises axin, APC, glycogen synthase kinase 3β (GSK-3β), and casein kinase 1 (CK1). [29] The kinases constituting the protein complex phosphorylate β-catenin. [30] Phosphorylated β-catenin is recognized and ubiquitinated by β-TrCP (β-transcriptase) and eventually degraded by the proteasome. [31] Recent studies have disclosed that the β-catenin regulation mechanism also acts on Ras (Fig. 2). [32] Ras interacts with β-catenin through an α-interface that includes Thr 144 and Thr 148, target sites of GSK-3β. [33] As β-catenin is removed from the binding site, the threonine residues are exposed, resulting in the phosphorylation and subsequent degradation of Ras. [33] This β-catenin dependent Ras degradation implies that Ras can be suppressed by stabilizing the destruction complex. [32].

In a previous study, we reported **KY1220** and its optimized compound, **KYA1797K (1)**. [34] The chemical structure of **1** has furan and rhodanine, which caused degradation of Ras through stabilization of the β-catenin destruction complex that resulted in an antitumor effect in the CRC model. Despite its promising antitumor activities, the furan/rhodanine moiety of **1** could cause poor physico-chemical properties. To improve the solubility, we designed a new series of analogs by modifying furan/rhodanine groups and conducted *in silico* binding affinity calculations between the designed compounds and axin (Fig. 3). After *in silico* analysis of the designed compounds, the furan/rhodanine moiety of **1** was replaced with pyridine/2,4-dioxothiazolidine (TZD) moiety. Furthermore, diverse substituents were introduced on the 3-nitrogen of TZD to improve the activities of the analogs.

2. Results

2.1. Chemistry

Synthetic routes for the new series of derivatives are depicted in Scheme 1 - 2. Most of the tested analogs were synthesized by the Knoevenagel condensation of aldehydes (**2**) and rhodanine and its analogs (**6**). As described in Scheme 1, the starting aryl aldehyde intermediates **2a - c** were prepared by the Suzuki reaction, whereas **2d** was synthesized through the *N*-arylation of pyrazole-3-carboxylate and subsequent reduction–oxidation reactions. *N*-functionalized TZD intermediates (**4** and **6**) were obtained through the following synthetic routes. The ester intermediates **3a**, **3c** were synthesized under nucleophilic substitution conditions, while **3b** was alternatively obtained via Michael reaction with methyl acrylate to avoid a possible elimination reaction. Ester intermediates **3** were hydrolyzed under acidic conditions to produce **6a – c**. Alcohol-containing intermediate **4** was directly

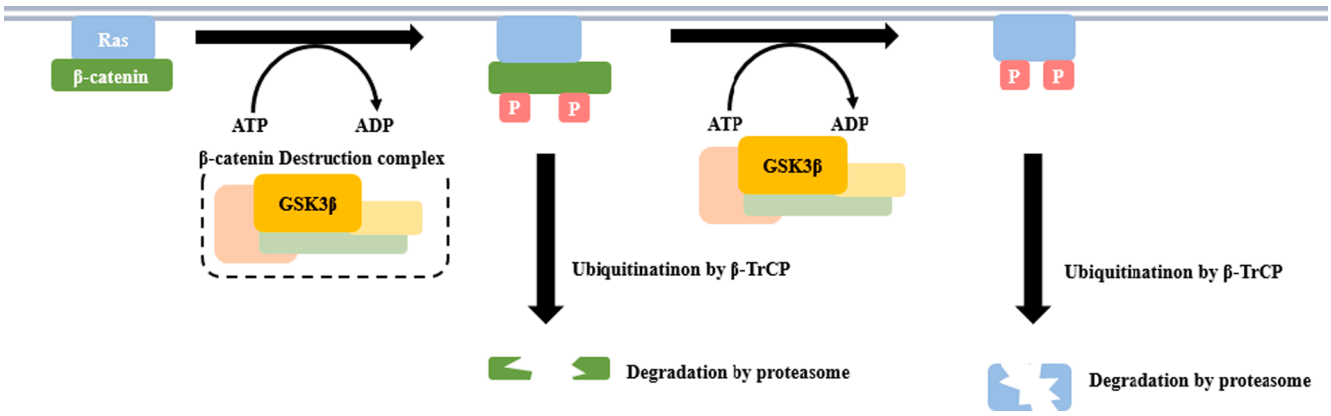

Fig. 2. Schematic representation for stepwise degradation of β-catenin and Ras by β-catenin destruction complex. [33] GSK-3β phosphorylates Ras bound β-catenin to induce β-TrCP mediated polyubiquitination and sequential degradation by proteasome. Remaining Ras is phosphorylated by GSK-3β and degraded through the same mechanism as β-catenin.

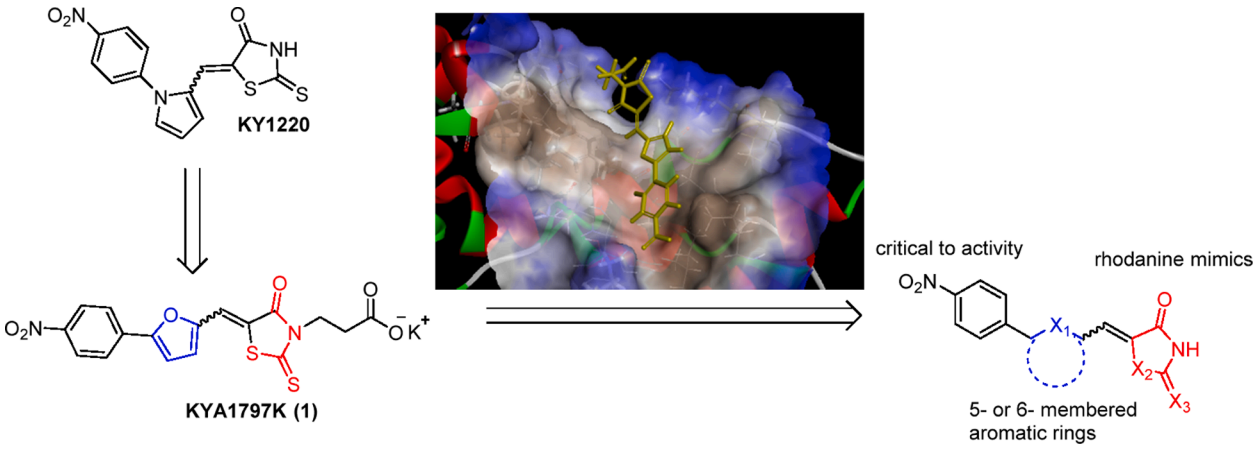

Fig. 3. Design strategy of **KYA1797K (1)** derivatives. Based on the binding mode of **1** to RGS domain of axin, design and optimization were performed to improve potency and solubility.

synthesized by a nucleophilic substitution reaction. For amine-containing intermediates synthesis (**6d – n**) the following reactions were performed, **5a** was produced by tosylation of **4a** and **5b** was obtained by direct reaction with 1,3-dibromopropane at the 3-nitrogen position of TZD. Intermediate **5** was reacted with the corresponding amines to afford the intermediates **6d – n**, and the resulting secondary amines in **6 m** and **6n** were Boc-protected to prepare **6o** and **6p** for the following reaction. The synthesis of derivatives of **1** is shown in Scheme 2. Aryl aldehydes **2a - d** with various aromatic rings were condensed with rhodanine and its analogs (**7**) such as hydantoin, thiohydantoin, and thiazolidine-2,4-dione (TZD) to acquire the targeted products with furan (**8a-d**), thiophene (**9a-d**), pyridine (**10a, 10b**), and pyrazole (**11a, 11b**) linkers under Knoevenagel conditions. The *N*-substituted TZD intermediates **4** and **6** were condensed with **2a** or **2c** to produce final compound **12** and **13** under the same conditions as described above. Among the final compounds, **13c** was further reacted to produce other analogs containing amides (**14a – c**). Finally, derivatives containing Boc-protected amines (**13 m–p, 14c**) were deprotected to afford the targeted analogs (**13q–t, 14d**).

Reagents and conditions (a) $Pd(PPh_3)_4$, K_2CO_3, toluene/EtOH, reflux. (b) i) Cs_2CO_3, $Cu(OAc)_2$-H_2O, DMF, 150 °C. ii) DIBAL-H, CH_2Cl_2, 0 °C - RT. iii) pyridinium chlorochromate (PCC), CH_2Cl_2, RT. (c) K_2CO_3, MeCN, reflux. (d) methyl acrylate, DABCO, MeCN, 60 °C. (e) HCl (35 % aq.), reflux. (f) $(iPr)_2EtN$, MeCN, 0 °C - RT. (g) 1,3-dibromopropane, K_2CO_3, MeCN, reflux. (h) TsCl, Et_3N, DMAP, CH_2Cl_2, 0 °C - RT. (i) corresponding amines, K_2CO_3, MeCN, reflux. (j) Boc_2O, DMAP, MeOH, reflux.

Reagents and conditions (a) piperidine, EtOH, reflux. (b) HCl (4 N in 1,4-dioxane), RT. (c) EDC-HCl, DMAP, $(iPr)_2EtN$, CH_2Cl_2, RT.

2.2. Design strategy, synthesis, and in vitro evaluation.

Although **1** showed promising antitumor effects, the poor physicochemical properties of this compound might impede its further development. To improve solubility while maintaining the activity, we conducted structural modifications based on the binding mode of **1** to axin. Fig. 4 shows the interaction between **1** and the axin-RGS domain (PDB ID:1DK8). As we previously found, the *p*-nitrophenyl moiety played an essential role in the binding of this compound to axin and its consequent activity through hydrogen bonding with Lys147 of axin.[34] Therefore, the nitro group was conserved during the structural optimization of the other parts. The phenyl group of Phe119 interacted with furan and rhodanine of **1** through π-interactions. Thus, heterocycles and rhodanine equivalents were introduced to maintain similar interactions with Phe119 in order to discover appropriate substituents for the constituents (**Table. S1** in supplementary information).

1 stabilized the β-catenin destruction complex to induce the degradation of β-catenin and subsequent degradation of Ras. [33] Because the

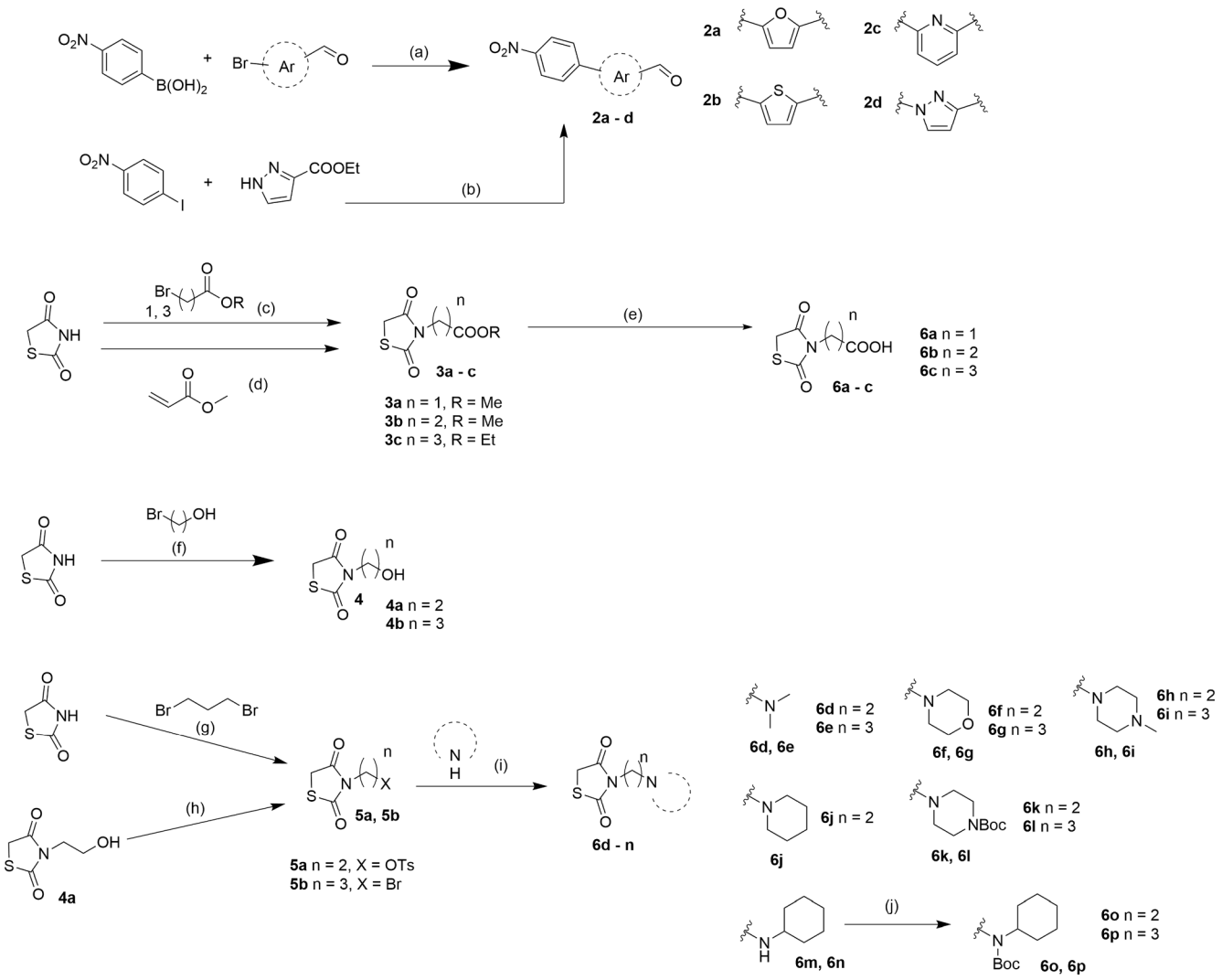

Scheme 1. Synthesis of Intermediates 2 – 6.

mechanism of action is dependent on β-catenin, the TOPflash assay (luciferase reporter gene assay) was the primary screening method to evaluate the effect of the compounds on the Wnt/β-catenin pathway. [35] In the TOPflash assay, reporter gene-transfected HEK293 cells were treated with Wnt3a-conditioned media (WntCM) in combination with DMSO, **1** as a positive control, or a newly prepared compound. Compounds showing significant inhibition in the TOPflash assay were immunoblotted to evaluate their effects on Ras and β-catenin levels in SW480 cells to identify the most potent compound among the synthesized derivatives.

Two sulfur atoms at the 1-position (X_1) and 2-thioxo (X_2) in the rhodanine ring of **1** presumably caused the poor physicochemical properties of this series of compounds. Therefore, the sulfur atoms at the X_1 and X_2 were replaced with nitrogen and oxygen, respectively. Compounds containing rhodanine or its equivalents (hydantoin, thiohydantoin, and 2,4-dioxothiazolidine (TZD)) were synthesized and evaluated as alternatives in a series of **8** and **9** (Table 1). In the results of **8**, hydantoin derivative (**8b**) showed fairly low inhibition of β-catenin even at a high concentration (10 μM). Analogs of thiohydantoin (**8a**), rhodanine (**8c**) and TZD (**8d**) showed similar activities and moderately inhibited β-catenin, with less than 40 % inhibition at 1 μM. For the analogs with a thiophene linker (**9**), thiohydantoin (**9a**) and hydantoin (**9b**) were barely active, while rhodanine (**9c**) and TZD (**9d**) showed good inhibition of β-catenin in a dose-dependent manner. Among the analogs, TZD derivative (**9d**), showed comparable activity to **1** at 1 μM (**9d**, 73 %, **1**, 72 % inhibition), was the most potent compounds (Table 1). Results of **8** and **9** indicated that it is difficult to replace the sulfur at X_1 position with nitrogen because the loss of π-interaction with Phe119 would cause a decrease in compound activity (Fig. 4). Meanwhile, the thioxo group of the rhodanine ring could be replaced with the oxo group (X_2 = O) because the analogs with TZD (**8d** and **9d**) showed comparable or better inhibition than rhodanine containing derivatives (**8c** and **9c**). Along with the above results, a further optimization was conducted by introducing pyridine and pyrazole linker in combination with rhodanine or TZD rings. In the pyridine linker, TZD analog (**10b**) showed significant inhibition (86 % inhibition at 1 μM). For pyrazole derivatives (**11**), rhodanine and TZD were both active at 1 μM (**11a**: 67 %, **11b**: 68 %). In summary, pyridine/TZD was found to be an adequate replacement for furan/rhodanine since **10b** was the most compound among the analogs **8 – 11** (Table. 1). Based on the result, further modification was performed at the 3-nitrogen position of the TZD. Considering that propionic acid group of **1** gave improvement of solubility, propionic acid group was introduced to **8d** and **10b** to examine potential improvement of furan/TZD (**12**) and pyridine/TZD (**13b**) derivatives.

Thus, the corresponding analogs of furan/TZD (**12**) and pyridine/

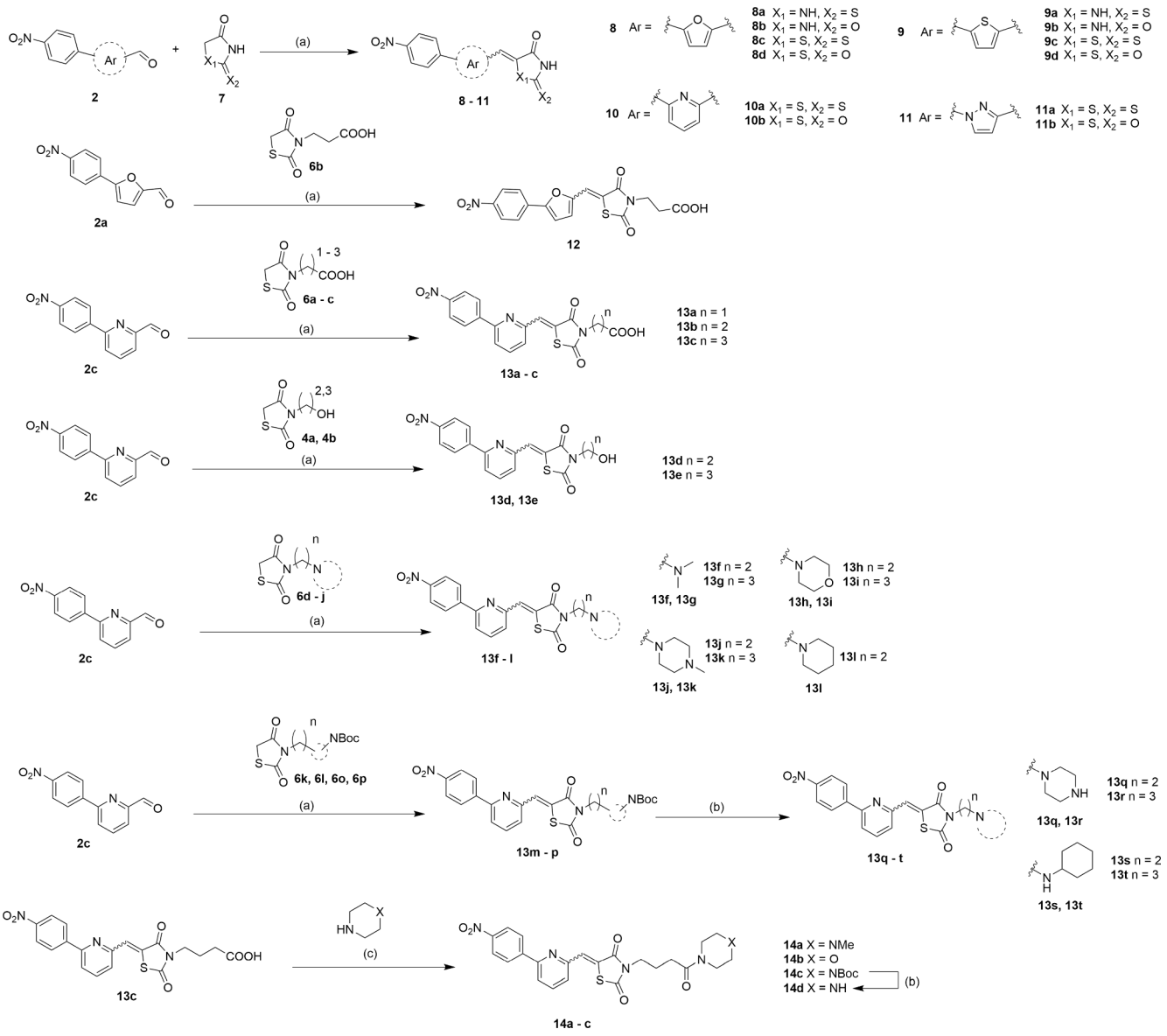

Scheme 2. Synthesis of target derivatives 8 – 14.

TZD (**13b**) with propionic acid were prepared to compare their solubility to **1** (Table. 2). As a result, **12** showed a remarkable improvement of solubility in PBS (12.25 ± 0.89 μg / mL) while its solubility in DW was still hardly soluble. Pyridine analog replacing of the original furan (**13b**) showed significant improvement of DW solubility (17.77 ± 0.29 μg / mL) and enhanced PBS solubility (19.90 ± 0.23 μg / mL). This result showed that the analogs of pyridine/TZD may give improvement of solubility. Although **13b** showed improved solubility, it had moderate activity. Therefore, diverse functional groups were introduced to enhance activity. Considering that propionic acid of **1** interacts with Lys126 of axin through polar interactions (Fig. 4), functional groups which are capable of the interaction (carboxylic acids, alcohols, amines, and amides) were introduced to substitute the moiety (**13**, **14**, Table. 3).

Carboxylic acids were preferentially introduced to improve aqueous solubility and *in vitro* activity. However, the corresponding derivatives **13a - c** did not show improved activity compared to the unsubstituted analog (**10b,** Table 1). The acetic acid derivative (**13a**) showed nearly no activity even at 10 μM, while the propionic (**13b**) and butanoic acid derivative (**13c**) recovered their activities at 10 μM and 5 μM, respectively. The absence of activity of **13a** may be caused by poor interaction of the acetate functional group with Lys126 of axin, while propionate and butanoate maintain the interaction (Fig. 4). As a result, the acetate analogs were excluded from further modification, and the activities at 1 μM were compared for the structure–activity relationship because the unsubstituted analog (**10b**) showed fairly good activity at 1 μM (Table. 1). When the alcohol functional group was introduced, **13d** and **13e** strongly inhibited β-catenin even at 1 μM (**13d**, **13e**: 98 % inhibition). For further optimization, various tertiary amines (*N,N*-dimethylamine, morpholine, piperidine, piperazine, *N*-methylpiperazine; **13f-r**) were introduced while primary amines were excluded for further modification because of their metabolic instability. As a result, most of the corresponding analogs showed weak inhibition at 1 μM, except for piperazine analogs (**13q** and **13r**) which showed moderate activity (**13q**: 52 %, **13r**: 58 % inhibition at 1 μM). The active piperazine analogs (**13q** and **13r)** have terminal secondary amines, which may form hydrogen bonds with axin. Therefore, other secondary amines with cyclohexyl groups (**13 s** and **13 t**) were additionally evaluated, but they also resulted in insignificant activity (**13 s**: 22 %, **13 t**: 18 % inhibition at

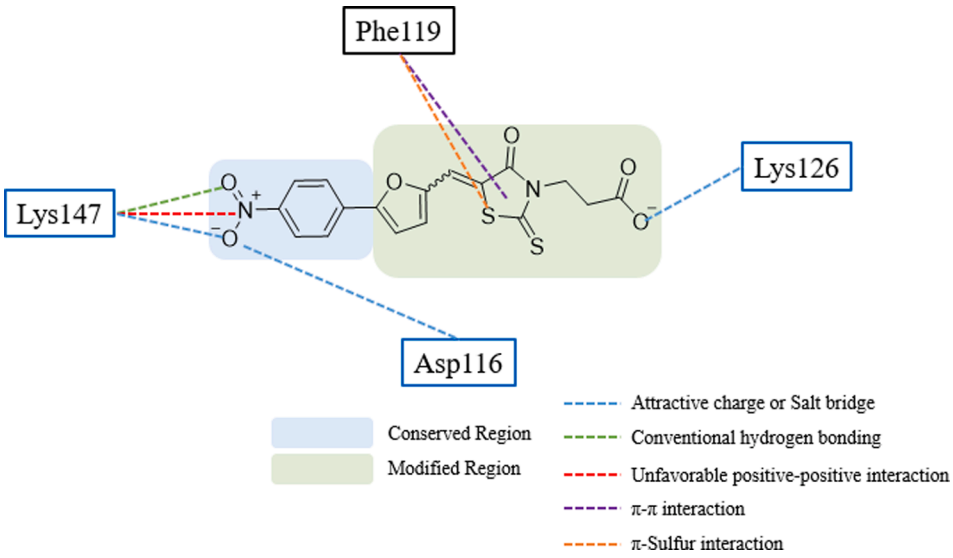

Fig. 4. Interaction between **1**-axin (1DK8). The *p*-nitrophenyl moiety was conserved because the polar interaction of the nitro group with Lys147 plays an essential role in compound activity. Furan/rhodanine was modified to improve solubility while maintaining π-interactions with Phe119. Polar functional groups can interact with Lys147 introduced at the 3-nitrogen position to further improve its properties.

Table 1

TOPflash reporter assay results of 8 – 11.

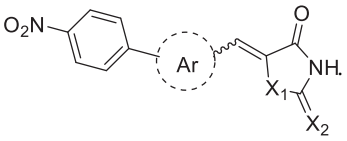

Cmpd#	Ar	X_1	X_2	Inhibition of β-catenin expression, [%] [a] (Normalized to WntCM + DMSO)		
				1 μM	5 μM	10 μM
1				71.84 ± 0.85	93.44 ± 1.00	93.87 ± 0.22
8a	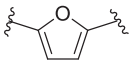	NH	S	37.48 ± 1.02	43.73 ± 0.74	52.13 ± 3.26
8b		NH	O	1.11 ± 3.72	9.44 ± 2.27	16.27 ± 4.47
8c		S	S	32.94 ± 1.75	66.97 ± 3.91	70.29 ± 0.15
8d		S	O	36.30 ± 3.32	56.59 ± 0.57	57.66 ± 0.58
9a	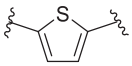	NH	S	2.57 ± 5.97	26.20 ± 5.99	42.03 ± 0.77
9b		NH	O	−2.57 ± 2.49	12.19 ± 1.06	28.25 ± 1.10
9c		S	S	23.53 ± 4.06	63.81 ± 1.56	79.76 ± 0.96
9d		S	O	73.28 ± 0.58	83.61 ± 0.65	89.86 ± 0.93
10a	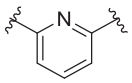	S	S	10.74 ± 6.28	67.63 ± 2.87	87.23 ± 0.06
10b		S	O	85.84 ± 1.10	91.54 ± 0.34	92.12 ± 0.17
11a	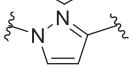	S	S	66.66 ± 1.73	93.50 ± 1.06	93.85 ± 0.01
11b		S	O	68.04 ± 0.49	93.08 ± 0.29	93.95 ± 0.17

a) Values are means of duplicates.

1 μM) because cyclohexyl groups may hinder hydrogen bonding with axin. For further modification of carboxylic acid, amide analogs (**14**) were prepared, and most of the analogs in this series showed weak inhibition at 1 μM, except for piperazine amide (**14d**), which has hydrogen bond donor (**14a**: 15 %, **14b**: not active, **14d**: 58 % inhibition at 1 μM).

Summarizing the structural optimization, pyridine linker and TZD ring were discovered as appropriate substituents for the furan linker and rhodanine ring, respectively. It was also found that the hydrogen bond donor in the TZD ring is critical for the activity. Among the prepared compounds, the alcohol containing analogs (**13d** and **13e**) showed improved inhibitory activity on β-catenin expression in compared with **1** (**13d**: 98 %, **13e**: 98 %, **1**–72 % inhibition at 1 μM).

Potent inhibitors, which have more than 85 % inhibition of β-catenin at 1 μM (**10b, 13d, 13e**), and moderately potent inhibitors, which have more than 80 % inhibition of β-catenin at 5 μM (**13f, 13 h, 13i, 13j, 14a**) in TOPflash assay (Table 1, 3), were immunoblotted to evaluate their effects of reducing pan-Ras and β-catenin levels in SW480 cells (Fig. 5). Although piperazine analogs (**13r** and **13 s**) had comparable activity to moderately potent compounds, **13r** showed cytotoxicity thus similar analogs (**13q**, **14d**) were also excluded in this assay. For evaluation, SW480 cells were treated with DMSO, **1** or the tested compounds at 5 and 25 μM concentration for 24 hr (Fig. 5A-C). The effects of these compounds on pan-Ras and β-catenin levels were compared with **1** by normalizing the protein levels (Fig. 5D). **10b** showed higher inhibition of pan-Ras, while the reduction in β-catenin level was less than **1** (Fig. 5A, D). Considering the mechanism of β-catenin-dependent degradation of the Ras protein,[33] **10b** is not considered a better inhibitor than **1**. The potent analogs (**13d** and **13e**), which exhibited strong inhibition of in the TOPflash reporter activity, exhibited a very potent reduction of the target proteins, while **13d** was considered as the better one (Fig. 5A, D). Other moderately potent inhibitors (**13f, 13 h, 13i, 13j, 14a**) showed similar activities to **1** except **13i**, which showed

Table 2
Solubility evaluation of **1, 12, 13b.**.

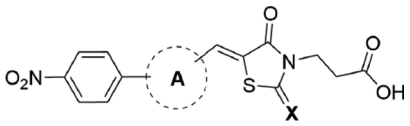

Cmpd [a]	A	X	Inhibition of β-catenin expression [%]			Solubility [b] [μg / mL]	
			1 μM	5 μM	10 μM	DW	PBS
1		S	71.84 ± 0.85	93.44 ± 1.00	93.87 ± 0.22	**less than 0.23**[c]	2.07 ± 0.14
12		O	58.58 ± 0.59	78.48 ± 0.62	86.44 ± 0.95	0.43 ± 0.04	12.25 ± 0.89
13b	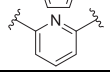	O	−1.86 ± 2.08	36.21 ± 2.16	74.92 ± 1.05	17.77 ± 0.29	19.90 ± 1.23

a) Compound solubility was evaluated in free form.
b) Values are means of duplicate.
c) Minimum concentration of concentration-UV absorbance curve.

better inhibition of Ras and β-catenin at 5 μM than **1**, but it was toxic at 25 μM (Fig. 5B – **D**). In summary, **13d** and **13e** were considered potential antitumor agents, and further evaluation of their colony formation assay on SW480 was performed.

The tumorigenesis of CRC is initiated by a loss-of-function mutation of *APC* and is further developed by Wnt/β-catenin pathway activation, which is induced by *KRAS* mutation. [36] The synergism of these two pathways induces the transformation of CRC cells to cancer stem cells, which causes chemoresistance and subsequent cancer recurrence. [37] Therefore, the inhibition of colony formation in SW480 cells with *APC*

Table 3
TOPflash assay results of **13, 14**.

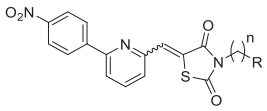

Cmpd#	n	R	Inhibition of β-catenin expression, [%] [a] (Normalized to WntCM + DMSO)		
			1 μM	5 μM	10 μM
1	2		71.84 ± 0.85	93.44 ± 1.00	93.87 ± 0.22
13a	1	COOH	1.85 ± 5.65	2.72 ± 5.51	11.98 ± 2.02
13b	2	COOH	−1.86 ± 2.08	36.21 ± 2.16	74.92 ± 1.05
13c	3	COOH	21.82 ± 3.70	76.43 ± 5.58	92.10 ± 2.51
13d	2	OH	98.56 ± 0.04	98.67 ± 0.04	99.07 ± 0.05
13e	3	OH	98.34 ± 0.04	98.67 ± 0.31	98.50 ± 0.02
13f	2		12.96 ± 2.12	84.80 ± 4.15	96.11 ± 0.78
13 g	3		1.16 ± 0.80	53.85 ± 0.53	89.09 ± 0.11
13 h	2		3.27 ± 5.68	77.75 ± 3.75	94.48 ± 1.97
13i	3		22.12 ± 12.41	89.18 ± 2.82	95.87 ± 1.04
13j	2		16.79 ± 6.56	87.65 ± 4.51	95.88 ± 0.55
13 k	3		3.85 ± 2.96	67.67 ± 3.04	88.62 ± 0.20
13 l	2		12.75 ± 6.04	30.93 ± 1.99	46.51 ± 1.54
13q	2		52.10 ± 1.89	94.58 ± 2.33	97.95 ± 0.11
13r	3		58.46 ± 0.33	96.02 ± 0.42	98.83 ± 0.17
13 s	2		21.52 ± 2.04	86.63 ± 1.34	98.11 ± 0.02
13 t	3		17.89 ± 2.15	88.72 ± 0.38	98.21 ± 0.06
14a	3	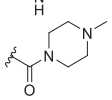	15.41 ± 7.50	89.56 ± 2.25	94.86 ± 0.12
14b	3		2.24 ± 3.71	42.86 ± 7.32	63.39 ± 2.05
14d	3	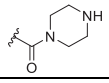	58.33 ± 3.61	96.53 ± 0.41	98.52 ± 0.27

a) Values are means of duplicate or triplicate.

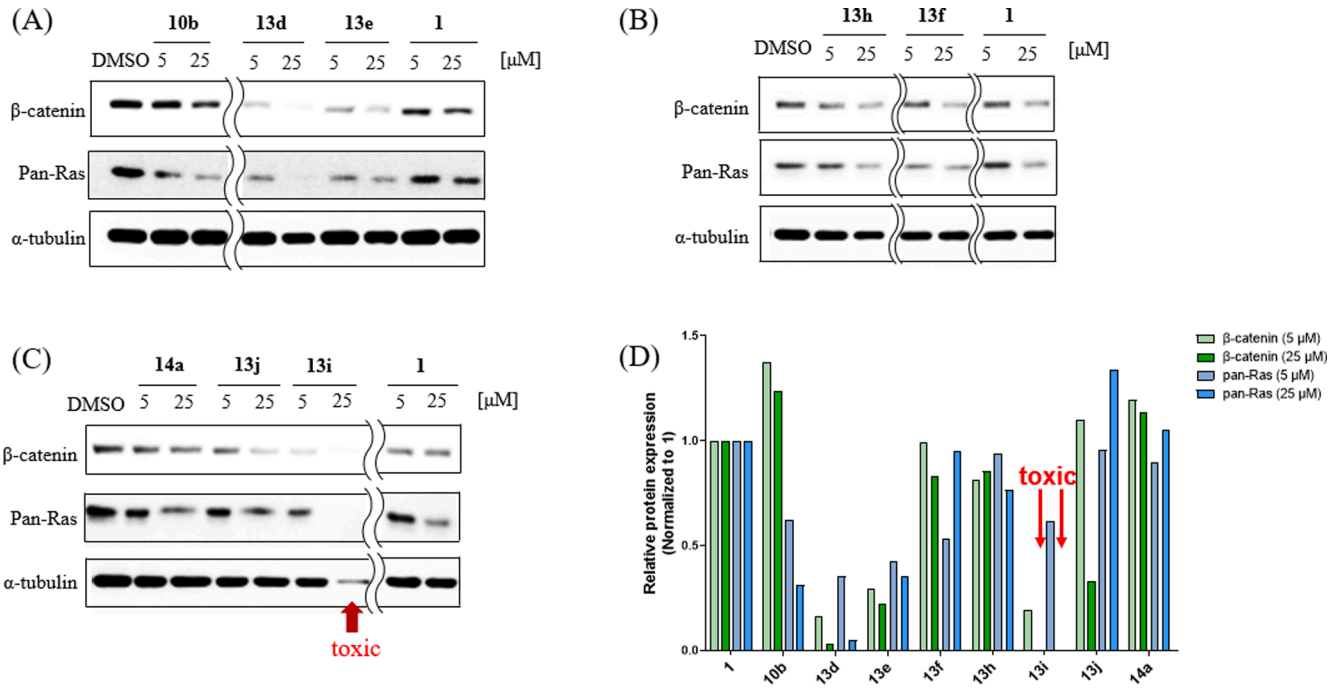

Fig. 5. Western blot results of active analogs (A – C). Effect of compounds (**10b**, **13d**, **13e**, **13f**, **13 h**, **13i**, **13j**, **14a**) on Ras and β-catenin level. SW480 was treated with **1** or selected compounds for 24 hr. (D) Relative Ras and β-catenin level after compound treatment. The protein expression was normalized to **1** to compare the effect of compounds.

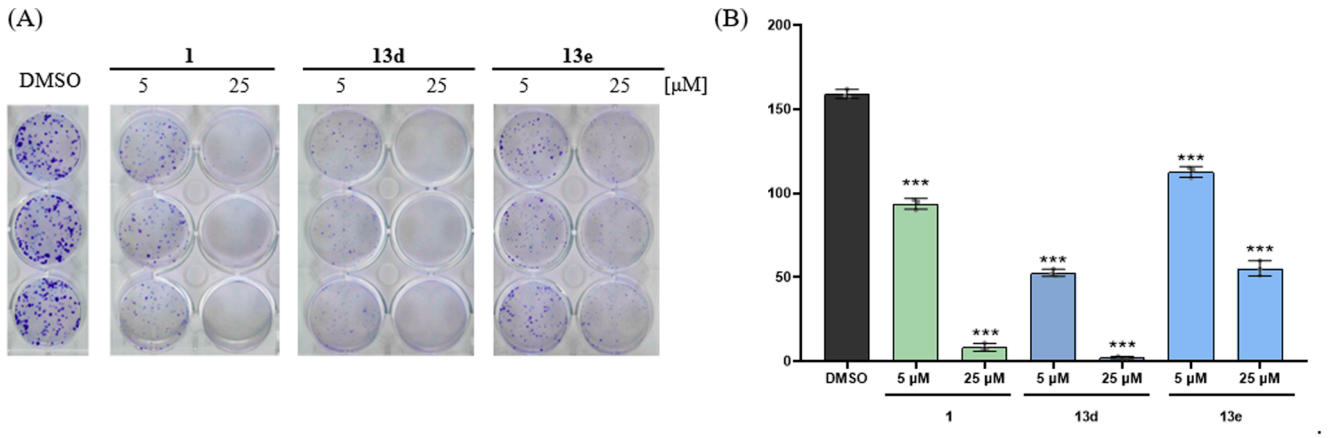

Fig. 6. Colony formation assay results. (A) Effects of **13d** and **13e** on SW480 colony formation in comparison with **1**. SW480 was treated with DMSO or selected compounds with concentrations of 5 μM and 25 μM until visible colonies formed. (B) Quantification of the colonies after treatment with potent compounds. The compounds caused a decrease in colony number in a dose-dependent manner. **13d** showed more potent inhibition on SW480 than **1**.

and *KRAS* mutations by the active compounds was examined for possible anti-CRC treatment. SW480 cells were treated with DMSO, **1**, **13d** or **13e** at concentrations of 5 or 25 μM every 3 days, and the number of colonies formed was counted (Fig. 6). All the compounds reduced the number of colonies in a dose-dependent manner (Fig. 6A). **13e** reduced 29 % of colonies at 5 μM and 66 % of colonies at 25 μM, which is less effective than **1,** which reduced the number of colonies by about 42 % and 95 % at 5 and 25 μM, respectively. However, **13d** resulted in more potent inhibition of colony formation at both concentrations (67 % and 99 % reduction at 5 μM and 25 μM) than **1** (Fig. 6B). Collectively, **13d** was identified as the most promising compound as a novel Ras modulator.

2.3. Validation of 13d-Axin binding and its binding mode.

According to the previous study, **1** stabilizes the β-catenin destruction complex by binding to the RGS domain of axin (74–220). The binding affinity of **1** was measured by observing a decrease in the fluorescence emitted as the RGS domain of axin to **1** ratio increased. [34] To calculate the binding affinity of **13d** with the same binding region, the RGS domain of axin was titrated with **1** or **13d** in various ratios, and the UV absorbance at 360 nm was measured (Fig. 6A). In the result, **13d** led to a decrease in the fluorescence absorbance as the domain-compound ratio increased. The binding affinity of **13d** to the RGS domain of axin was slightly higher than that of **1** (**13d**, $K_d = 7.41E^{-07}$ M; **1**, $K_d = 9.02E^{-07}$ M). Fig. 7B and 7C describe the binding mode of **13d** with axin-RGS (PDB ID:1DK8). Similar to **1**, the nitro group of **13d**

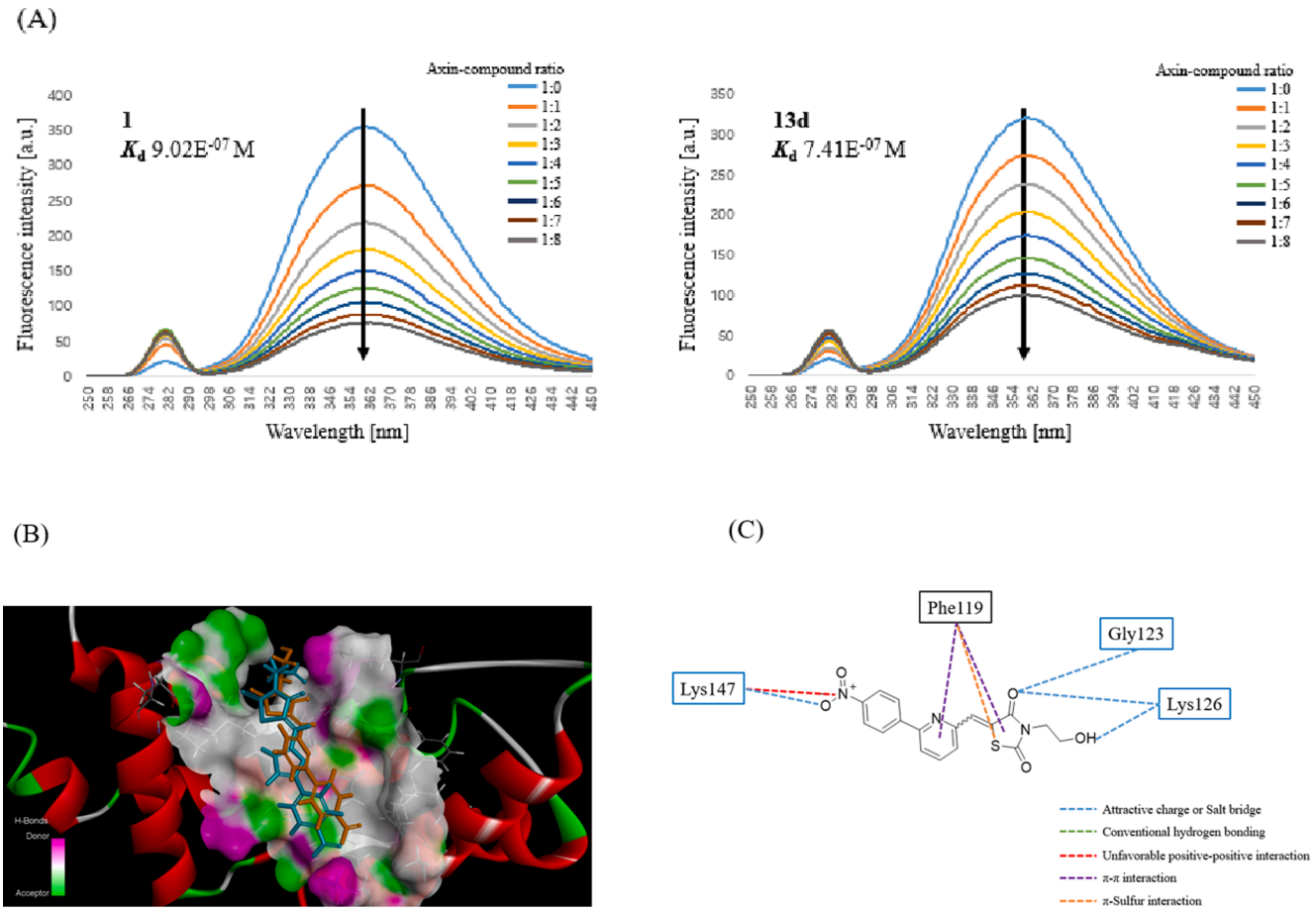

Fig. 7. (A) Fluorescence spectroscopy of **1** and **13d**. The compound-axin binding was validated through the decrease in UV absorbance in 360 nm wavelength from the binding target (Axin 74–220 (RGS domain of axin)) as the ratio of compound to target increases. Binding affinities (K_d) were calculated from fluorescence intensity according to the presence or absence of compounds. (B) Docking position of **13d** in comparison with **1**. (C) Binding mode of **13d**. The core interactions with Lys147, Phe119, and Lys126 of axin were conserved in **13d**-axin binding.

interacts with Lys147 through polar interactions. The pyridine-TZD group that substituted the furan-rhodanine group retained π-interactions with Phe119. The alcohol at the 3-position of TZD formed a hydrogen bond with Lys126, which interacted with the carboxylic acid of **1** (Fig. 4). Additionally, Lys126 can form another hydrogen bond with the 4-oxo group of TZD. Based on these results, **compound 13d** induced the intended mechanism of action by conserving the overall interaction with the RGS domain of axin.

3. Conclusion

Because mutations in Ras are closely related to tumorigenesis in various cancers, there is a tremendous unmet need for the development of Ras inhibitors. In this study, a series of compounds was designed and identified as degraders of Ras by harnessing the interaction between Ras and the Wnt/β-catenin pathway. The previously discovered compound **KYA1797K (1)** induced the simultaneous degradation of Ras and β-catenin through stabilization of the β-catenin destruction complex. To improve solubility of **1**, we designed a series of compounds using *in silico* docking approach to examine the binding mode of axin and the designed analogs and synthesized the proposed compounds. This modification replaced the rhodanine and furan linkers with TZD and pyridine to improve solubility, respectively (**10b**). Further optimization of **10b** introduced various functional groups at the 3-nitrogen position of TZD. As a consequence of the structural optimization, 3-(2-hydroxyethyl)-5-((6-(4-nitrophenyl)pyridin-2-yl)methylene) thiazolidine-2,4-dione (**13d**) was identified as the most potent compound. **13d** showed a remarkable reduction in Ras along with β-catenin. It also strongly inhibited clonogenicity in SW480 cells. The binding affinity of **13d** to the RGS domain of axin was slightly higher than that of **1**, suggesting that **13d** and **1** have the same binding mode as the RGS domain of axin. These results suggest that further development of **13d** could contribute to the development of Ras inhibitors with novel mechanisms of action.

4. Experimental protocol

4.1. General synthetic materials and methods

Commercial solvents and reactants were purchased from Alfa Aesar (US) and the Tokyo Chemical Industry (Japan), respectively. All purchased chemicals were used for the reaction without further purification. The reaction progress was monitored by thin layer chromatography (TLC), which was performed on silica gel 60G F254 plates (Merck, Germany) and visualized under 254 nm ultraviolet light. Column chromatography was performed using silica (Merck EM9385, 230 – 400 mesh, Germany). The synthesized compounds were identified using nuclear magnetic resonance (NMR) spectroscopy, low-resolution liquid chromatography/mass spectrometry (LRMS), and high-resolution liquid chromatography/mass spectrometry with an electrospray ionization probe (HRMS-ESI). ^{1}H and ^{13}C NMR spectroscopy was performed using an Avance II NMR spectrometer (Bruker Biospin, Germany), and the spectra were recorded at 400 MHz and 100 MHz, respectively. NMR chemical shifts are expressed in parts per million (ppm) relative to trimethylsilane (TMS), which is contained in deuterated solvents as an

internal standard. The coupling constant (*J*) of ^{1}H NMR is expressed in hertz, and the splitting patterns of ^{1}H NMR shifts are expressed as follows: s, singlet; d, doublet; t, triplet; q, quartet; m, multiplet (for peaks split into five or more branches or have ambiguous shapes); br s, broad singlet. LRMS was performed using a Shimadzu LCMS-2020 instrument (Shimadzu Corporation, Japan). Compound validation through LRMS analysis was performed by detecting integer values corresponding to [M + H] in the positive probe or [M−H] in the negative probe, where M is the compound's molecular weight. HRMS was performed using an Agilent 6530 Accurate-Mass Quadrupole Time-of-Flight (Q-TOF) system (Agilent, US). The molecular weight of the synthesized compound was confirmed by detecting the corresponding positive [M + H] or negative [M−H] ion peaks with error values less than 0.1 with calculated [M + z]/z or [M−z]/z, where M represents the exact mass of the compound and z is the proton. The purity of the final compounds were calculated based on UV absorbance obtained through high-performance liquid chromatography (HPLC). HPLC analysis was performed on Shimadzu HPLC instrument (Shimadzu, Japan) using Agilent ZORBAX Eclipse Plus C18 (95 Å, 4.6 × 150 mm, 5 μM), mobile phase; acetonitrile and water, both containing 0.05 % formic acid.

5-(4-nitrophenyl)furan-2-carbaldehyde (**2a)** was purchased from Tokyo Chemical industry (TCI) and used for reactions without further purification.

5-(4-nitrophenyl)thiophene-2-carbaldehyde (**2b**). To a mixture of 5-bromothiophene-2-carbaldehyde (1.03 g, 5.38 mmol) and 4-nitrophenylboronic acid (0.99 g, 5.92 mmol) in toluene/EtOH (1:1), tetrakis (triphenylphosphine)palladium(0) (310 mg, 0.27 mmol), and K_2CO_3 (1.45 g, 10.76 mmol) were added. The reaction mixture was heated to 100 °C for 16 h and cooled to RT. The mixture was then condensed under reduced pressure and extracted with ethyl acetate (EtOAc). The combined organic layers were dried over sodium sulfate and filtered. The filtrate was concentrated under reduced pressure and purified by flash column chromatography (EtOAc/*n*-hexane = 1:5 – 1:3) to afford the title intermediate **2b** (702 mg, 56 %) as a yellow solid. ^{1}H NMR (400 MHz, DMSO-d_6) δ 9.97 (s, 1H), 8.32–8.30 (m, 2H), 8.13–8.09 (m, 3H), 8.00–7.99 (m, 1H).

6-(4-nitrophenyl)pyridine-2-carbaldehyde (**2c**). Following the procedure for **2b**, 5-bromopyridine-2-carbaldehyde (1.20 g, 6.45 mmol) was used to afford **2c** (545 mg, 37 %) as a pale yellow solid. ^{1}H NMR (400 MHz, DMSO-d_6) δ 10.10–10.10 (m, 1H), 8.50–8.39 (m, 5H), 8.26–8.22 (m, 1H), 8.02–7.99 (m, 1H).

1-(4-nitrophenyl)pyrazole-3-carbaldehyde (**2d**)**.** To a solution of ethyl pyrazole-3-carboxylate (1.50 g, 10.70 mmol) and 4-iodonitrobenzene (2.80 g, 11.24 mmol) in DMF, Cs_2CO_3 (4.53 g, 13.92 mmol) and Cu $(OAc)_2$-H_2O (107 mg, 0.54 mmol) were added and then the mixture was heated at 150 °C for 16 h. After product formation was confirmed by thin-layer chromatography (TLC), the mixture was cooled to RT. An excess amount (x20 volume of DMF) of water was poured onto the crude reaction mixture, filtered, and washed with water and dried. The collected precipitate was dissolved in dichloromethane and the solution was cooled to 0 °C. To the solution, DIBAL-H (32.10 mmol, 1 M in *n*-hexane) was slowly added and stirred for 16 h while being slowly warmed to RT. After reaction completion, distilled water and NaOH (15 wt% in H_2O) were sequentially added and stirred for 15 min to quench the remaining reagent, followed by the addition of sodium sulfate and filtered. The crude residue was evaporated under reduced pressure and solvated with dichloromethane. To the mixture, PCC (6.92 g, 30.10 mmol) was then added, and the mixture was stirred at RT for 3 h. After the reaction was complete, an excess amount of diethyl ether was poured into the reaction mixture and filtered. The residue was collected, condensed under reduced pressure, and purified by column chromatography (1:5 to 1:3 EtOAc / *n*-hexane) to afford the title intermediate **2d** (1.32 g, 57 %) as a pale yellow solid. ^{1}H NMR (400 MHz, DMSO-d_6) δ 10.05 (s, 1H), 8.91–8.90 (m, 1H), 8.44–8.42 (m, 2H), 8.25–8.23 (m, 2H), 7.14–7.13 (m, 1H).

Methyl 2-(2,4-dioxothiazolidin-3-yl)acetate (**3a**). To a mixture of 2,4-dioxothiazolidine (562 mg, 4.80 mmol), methyl bromoacetate (0.53 mL, 5.76 mmol) in ACN solution, K_2CO_3 (796 mg, 5.76 mmol) was added. The reaction mixture was then refluxed for 16 h and cooled to RT. The reaction mixture was concentrated under reduced pressure then extracted with dichloromethane. The collected organic phase was dried over sodium sulfated and filtered. The filtrate was evaporated under reduced pressure and purified by flash column chromatography (EtOAc / *n*-hexane = 1:3) to afford **5a** (415 mg, 45 %) as a colorless oil. ^{1}H NMR (400 MHz, DMSO-d_6) δ 4.35 (s, 2H), 4.34 (s, 2H), 3.69 (s, 3H).

Methyl 3-(2,4-dioxothiazolidin-3-yl)propanoate (**3b**) A mixture of 2,4-dioxothiazolidine (577 mg, 4.93 mmol), 1,4-diazabicyclo[2.2.2]octane (276 mg, 2.46 mmol) and the methyl acrylate (0.67 mL, 7.39 mmol) was dissolved in ACN. The solution was heated at 60 °C for 16 h. The reaction mixture was then cooled to RT and evaporated under reduced pressure. The residue was purified by column chromatography (EtOAc / *n*-hexane = 1:3) to obtain **3b** (460 mg, 46 %) as a colorless oil. ^{1}H NMR (400 MHz, DMSO-d_6) δ 4.18 (s, 2H), 3.73 (t, 2H, J = 7.2 Hz), 3.59 (s, 3H), 2.57 (t, 2H, J = 7.6 Hz).

Ethyl 4-(2,4-dioxothiazolidin-3-yl)butanoate (**3c**) Following the procedure of **3a**, ethyl 4-bromobutanoate (965 mg, 4.95 mmol) was used to afford **3c** (561 mg, 58 %) as a colorless oil. ^{1}H NMR (400 MHz, DMSO-d_6) δ 4.16 (s, 2H), 4.04 (q, 2H, J = 7.2 Hz), 3.52 (t, 2H, J = 6.8 Hz), 2.31 (t, 2H, J = 7.2 Hz), 1.78–1.71 (m, 2H), 1.18 (t, 3H, J = 6.8 Hz).

3-(2-hydroxyethyl)thiazolidine-2,4-dione (**4a**). To a solution of 2,4-dioxothiazolidine (504 mg, 4.30 mmol) and 2-bromoethanol (0.46 mL, 6.46 mmol) in ACN, a solution of $(iPr)_2$EtN (1.50 mL, 8.61 mmol) in ACN was slowly added over 30 min. The reaction solution was stirred for 16 h while being slowly warmed to RT from 0 °C. After the reaction, the solution was evaporated under reduced pressure and purified by flash column chromatography (EtOAc / *n*-hexane = 1:3) to afford the title intermediate **4a** (693 mg, 45 %) as a yellow oil. ^{1}H NMR (400 MHz, DMSO-d_6) δ 4.84 (t, 1H, J = 5.6 Hz), 4.16 (s, 2H), 3.58–3.54 (m, 2H), 3.51–3.47 (m, 2H).

3-(3-hydroxypropyl)thiazolidine-2,4-dione (**4b**). Following the same procedure of **4a**, 3-bromopropanol (0.54 mL, 6.21 mmol) was used to afford **4b** (283 mg, 39 %) as a colorless oil. ^{1}H NMR (400 MHz, DMSO-d_6) δ 4.55 (t, 1H, J = 5.2 Hz), 4.18 (s, 2H), 3.56–3.52 (m, 2H), 3.40 (q, 2H, J = 6.4 Hz), 1.66–1.59 (m, 2H).

2-(2,4-dioxothiazolidin-3-yl)ethyl 4-methylbenzenesulfonate (**5a**). To a solution of **4a** (545 mg, 3.38 mmol) in CH_2Cl_2, *p*-toluenosulfonyl chloride (967 mg, 5.07 mmol) and 4-dimethylaminopyridine (41 mg, 0.34 mmol) were added followed by slow addition of Et_3N (0.94 mL, 6.76 mmol) over 20 min. The reaction mixture was stirred for 16 h while slowly warming to RT from 0 °C. After the formation of the product was confirmed, the reaction solution was evaporated under reduced pressure and purified by flash column chromatography (EtOAc / *n*-hexane = 1:5 ~ 1:1) to obtain the title intermediate **5a** (855 mg, 80 %) as a yellow solid. ^{1}H NMR (400 MHz, DMSO-d_6) δ 7.74–7.72 (m, 2H), 7.51–7.49 (m, 2H), 4.16 (t, 2H, J = 4.8 Hz), 4.10 (s, 2H), 3.73 (t, 2H, J = 5.2 Hz), 2.43 (s, 3H).

3-(3-bromopropyl)thiazolidine-2,4-dione (**5b**). To a solution of 2,4-dioxothiazolidine (2.16 g, 18.45 mmol) in ACN, 1,3-dibromopropane (2.80 mL, 27.68 mmol) and K_2CO_3 (5.10 g, 36.90 mmol) were added. The reaction mixture was refluxed for 16 h. After the reaction, the mixture was concentrated under reduced pressure and extracted with dichloromethane. The collected organic layers were dried over sodium sulfate and filtered. The filtrate was evaporated under reduced pressure and purified by flash column chromatography (EtOAc / *n*-hexane = 1:3) to afford the title intermediate **5b** (1.33 g, 30 %) as a colorless oil. ^{1}H NMR (400 MHz, DMSO-d_6) δ 4.16 (s, 2H) 3.61 (t, 2H, J = 6.8 Hz), 3.51 (t, 2H, J = 6.4 Hz), 2.07–2.01 (m, 2H).

2-(2,4-dioxothiazolidin-3-yl)acetic acid (**6a**). HCl (35 %) was poured to **3a** (754 mg, 3.99 mmol) and the reaction mixture was refluxed for 16 h. After the reaction, the mixture was evaporated under reduced pressure and purified by flash column chromatography (2 % MeOH /CH_2Cl_2) to afford the title intermediate **6a** as a white solid (514 mg, 73 %). ^{1}H

NMR (400 MHz, DMSO-d_6) δ 4.33 (s, 2H), 4.20 (s, 2H).

3-(2,4-dioxothiazolidin-3-yl)propanoic acid (**6b**). Following the procedure of **6a**, **3b** (559 mg, 2.75 mmol) was used to obtain **6b** as a white solid (350 mg, 67 %). ^{1}H NMR (400 MHz, DMSO-d_6) δ 4.16 (s, 2H), 3.70 (t, 2H, J = 7.6 Hz), 2.49 (t, 2H, J = 7.6 Hz).

4-(2,4-dioxothiazolidin-3-yl)butanoic acid (**6c**). Following the procedure of **6a**, **3c** (3.20 g, 13.84 mmol) was used to obtain **4a** as a white solid (1.80 g, 64 %). ^{1}H NMR (400 MHz, DMSO δ 4.16 (s, 2H), 3.52 (t, 2H, J = 6.8 Hz), 2.22 (t, 2H, J = 7.6 Hz), 1.76–1.68 (m, 2H).

General procedure 1 (GP1) for synthesis of **6d – n**. To a solution of **4** in ACN, the corresponding amine (3 equiv.), and K_2CO_3 (1.2 equiv.) were added, and the reaction mixture was refluxed for 16 h. After reaction completion was confirmed by TLC, the mixture was cooled to RT, evaporated under reduced pressure, and extracted with CH_2Cl_2 three times. The collected organic layers were dried over sodium sulfate, filtered and evaporated under reduced pressure. The title intermediate was obtained through flash column chromatography (**6d - l**, (EtOAc / *n*-hexane = 1:1 ~ 5 % MeOH / CH_2Cl_2)) or used for next reaction without further purification (**6 m, 6n**).

3-(2-(dimethylamino)ethyl)thiazolidine-2,4-dione (**6d**). Following the *GP1*, **4a** (520 mg, 1.65 mmol) and dimethylamine (8 % in ACN, 1 mL) were used to afford **6d** (149 mg, 48 %) as a brown oil. ^{1}H NMR (400 MHz, DMSO-d6) δ 4.21 (s, 2H), 3.58 (t, 2H, J = 6.4 Hz), 2.38 (t, 2H, J = 6.4 Hz), 2.14 (s, 6H).

3-(3-(dimethylamino)propyl)thiazolidine-2,4-dione (**6e**). Following the *GP1*, **4b** (490 mg, 2.06 mmol) and dimethylamine (8 % in ACN, 1 mL) were used to afford **6e** (207 mg, 50 %) as a yellow oil. ^{1}H NMR (400 MHz, DMSO-d6) δ 4.17 (s, 2H), 3.51 (t, 2H, J = 7.2 Hz), 2.19 (t, 2H, J = 7.2 Hz), 2.10 (s, 6H), 1.64–1.57 (m, 2H).

3-(2-morpholinoethyl)thiazolidine-2,4-dione (**6f**). Following the *GP1*, **4a** (320 mg, 1.02 mmol) and morpholine (0.26 mL, 3.04 mmol) were used to afford **6f** (151 mg, 64 %) as an orange oil. ^{1}H NMR (400 MHz, DMSO-d_6) δ 4.21 (s, 2H), 3.61 (t, 2H, J = 6.8 Hz), 3.52–3.50 (m, 4H), 2.42 (t, 2H, J = 6.4 Hz), 2.37 (s, 4H).

3-(3-morpholinopropyl)thiazolidine-2,4-dione (**6 g**). Following the *GP1*, **4b** (201 mg, 0.84 mmol) and morpholine (0.22 mL, 2.53 mmol) were used to afford **6 g** (185 mg, 90 %) as an orange solid. ^{1}H NMR (400 MHz, DMSO-d_6) δ 4.17 (s, 2H), 3.56–3.53 (m, 6H), 2.28–2.25 (m, 6H), 1.68–1.61 (m, 2H).

3-(2-(4-methylpiperazin-1-yl)ethyl)thiazolidine-2,4-dione (**6 h**). Following the *GP1*, **4a** (451 mg, 1.43 mmol) and 1-methylpiperazine (0.48 mL, 4.29 mmol) were used to afford **6 h** (160 mg, 45 %) as an orange oil. LRMS (ESI) 244 $[M + H]^+$ was detected; ^{1}H NMR (400 MHz, DMSO-d_6) δ 4.20 (s, 2H), 3.59 (t, 2H, J = 6.4 Hz), 2.43–2.18 (m, 10*H*), 2.13 (s, 3H).

3-(3-(4-methylpiperazin-1-yl)propyl)thiazolidine-2,4-dione (**6i**). Following the *GP1*, **4b** (490 mg, 2.06 mmol) and 1-methylpiperazine (0.46 mL, 4.12 mmol) were used to afford **6i** (380 mg, 72 %) as a brown oil. ^{1}H NMR (400 MHz, DMSO-d_6) δ 4.16 (s, 2H), 3.52 (t, 2H, J = 7.2 Hz), 2.29–213 (m, 10*H*), 2.13 (s, 3H), 1.66–1.59 (m, 2H).

3-(2-(piperidin-1-yl)ethyl)thiazolidine-2,4-dione (**6j**). Following the *GP1*, **4a** (100 mg, 0.32 mmol) and piperidine (94 μL, 0.95 mmol) were used to afford **6j** (72 mg, 61 %) as an orange oil. ^{1}H NMR (400 MHz, DMSO-d_6) δ 4.20 (s, 2H), 3.59 (t, 2H, J = 6.8 Hz), 2.40–2.33 (m, 6H), 1.46–1.34 (m, 6H).

Tert-butyl 4-(2-(2,4-dioxothiazolidin-3-yl)ethyl)piperazine-1-carboxylate (**6 k**). Following the *GP1*, **4a** (200 mg, 0.63 mmol) and 1-Bocpiperazine (354 mg, 1.90 mmol) were used to afford **6 k** (174 mg, 83 %) as a brown oil. ^{1}H NMR (400 MHz, DMSO-d_6) δ 4.21 (s, 2H), 3.61 (t, 2H, J = 6.4 Hz), 3.25–3.24 (m, 4H), 2.44 (t, 2H, J = 6.4 Hz), 2.34–2.32 (m, 4H), 1.38 (s, 9H).

Tert-butyl 4-(3-(2,4-dioxothiazolidin-3-yl)propyl)piperazine-1-carboxylate (**6 l**). Following the *GP1*, **4b** (269 mg, 1.13 mmol) and 1-Bocpiperazine (631 mg, 3.39 mmol) were used to afford **6 l** (352 mg, 90 %) as a pale brown oil. ^{1}H NMR (400 MHz, DMSO-d_6) δ 4.17 (s, 2H), 3.54 (t, 2H, J = 6.8 Hz), 3.29–3.28 (m, 4H), 2.29–2.22 (m, 6H), 1.68–1.62 (m, 2H).

3-(2-(cyclohexylamino)ethyl)thiazolidine-2,4-dione (**6 m**). Following the *GP1*, **4a** (578 mg, 1.83 mmol) and cyclohexylamine (0.63 mL, 5.50 mmol) were used to afford a crude of **9 g**. The obtained crude was used for next reaction without further purification.

3-(3-(cyclohexylamino)propyl)thiazolidine-2,4-dione (**6n**). Following the *GP1*, **4b** (642 mg, 2.67 mmol) and cyclohexylamine (0.92 mL, 8.01 mmol) were used to afford a crude of **6n**. The obtained crude was used for next reaction without further purification.

Tert-butyl cyclohexyl(2-(2,4-dioxothiazolidin-3-yl)ethyl)carbamate (**6o**). To a solution of crude **6 m** and 4-dimethylaminopyridine (67 mg, 0.55 mmol) in MeOH, di(*tert*-butyl) dicarbonate (1.20 g, 5.50 mmol) in MeOH was added slowly at RT. The solution was refluxed for 16 h then cooled to RT and evaporated under reduced pressure. The obtained residue was purified through flash column chromatography (EtOAc / *n*-hexane = 1:3) to produce 6o (120 mg, 19 % over 2 steps) as a yellow oil. LRMS (ESI) *m/z* 343 $[M + H]^+$, 243 $[M-Boc + H]^+$ were detected.

Tert-butyl cyclohexyl(3-(2,4-dioxothiazolidin-3-yl)propyl)carbamate (**6p**). Following the procedure of **6o**, **6n** was used to produce **6p** (190 mg, 20 % over 2 steps) as a yellow oil. ^{1}H NMR (400 MHz, DMSO-d_6) δ 4.20 (s, 2H), 3.47 (t, 2H, J = 7.2 Hz), 1.75–1.63 (m, 5H), 1.58–1.55 (m, 4H), 1.36 (s, 10*H*), 1.28–1.18 (m, 3H), 1.11–1.04 (m, 2H).

General procedure 2 (GP2) for synthesis of **8 – 13.** To a suspension of **2** (1.0 equiv.) in EtOH, **4**, **6** or **7** (1.2 equiv.), and piperidine (1.2 equiv.) was added, and the mixture was refluxed for 16 h. After completion of the reaction, the mixture was cooled to RT, filtered, and washed with EtOH and diethyl ether (Et_2O) to collect the precipitate as title compounds **8 – 13**.

5-((5-(4-nitrophenyl)furan-2-yl)methylene)-2-thioxoimidazolidin-4-one (**8a**). Following the *GP2*, **2a** (100 mg, 0.46 mmol) and 2-thiohydantoin (64 mg, 0.55 mmol) were used to afford **8a** (138 mg, 95 %) as an orange powder. ^{1}H NMR (400 MHz, DMSO-d_6) δ 12.26 (br s, 1H), 8.30–8.27 (m, 2H), 8.18–8.15 (m, 2H), 7.49–7.48 (m, 1H), 7.36–7.35 (m, 1H), 6.42 (s, 1H); ^{13}C NMR (100 MHz, DMSO-d_6) δ 178.9, 165.9, 154.0, 151.2, 146.8, 135.4, 126.5, 125.7, 124.7, 119.1, 114.0, 98.6; HRMS (ESI): calculated for $C_{14}H_9N_3O_4S$, 314.0236 $[M-H]^-$; found, 314.0227; HPLC analysis 98.47 % (R_t: 12.86 min).

5-((5-(4-nitrophenyl)furan-2-yl)methylene)imidazolidine-2,4-dione (**8b**). Following the *GP2*, **2a** (100 mg, 0.46 mmol) and hydantoin (55 mg, 0.55 mmol) were used to afford **8b** (82 mg, 60 %) as a maroon powder. ^{1}H NMR (400 MHz, DMSO-d_6) δ 8.22–8.19 (m, 2H), 8.11–8.08 (m, 2H), 7.39–7.39 (m, 1H), 7.08–7.07 (m, 1H), 6.30 (s, 1H); ^{13}C NMR (100 MHz, DMSO-d_6) δ 165.7, 156.0, 152.9, 151.7, 146.5, 135.6, 127.4, 125.3, 124.6, 116.7, 113.6, 96.1; HRMS (ESI): calculated for $C_{14}H_9N_3O_5$, 298.0464 $[M-H]^-$; found, 298.0456; HPLC analysis 94.93 % (R_t: 11.52 min).

5-((5-(4-nitrophenyl)furan-2-yl)methylene)-2-thioxothiazolidin-4-one (**8c**). Following the *GP2*, **2a** (126 mg, 0.58 mmol) and rhodanine (92 mg, 0.70 mmol) were used to afford **8c** (138 mg, 72 %) as an orange powder. ^{1}H NMR (400 MHz, DMSO-d_6) δ 13.77 (br s, 1H), 8.41–8.38 (m, 2H), 8.06–8.03 (m, 2H), 7.60–7.59 (m, 1H), 7.53 (s, 1H), 7.37–7.36 (m, 1H); ^{13}C NMR (100 MHz, DMSO-d_6) δ 196.7, 169.5, 155.5, 151.3, 147.3, 134.8, 125.5, 125.3, 124.4, 122.7, 117.2, 114.2; HRMS (ESI): calculated for $C_{14}H_8N_2O_4S_2$ 330.9847 $[M-H]^-$; found, 330.9850; HPLC analysis 97.67 % (R_t: 5.63 min).

5-((5-(4-nitrophenyl)furan-2-yl)methylene)thiazolidine-2,4-dione (**8d**). Following the *GP2*, **2a** (100 mg, 0.46 mmol) and 2,4-dioxothiazolidine (64 mg, 0.55 mmol) were used to afford **8d** (137 mg, 94 %) as a yellow powder. ^{1}H NMR (400 MHz, DMSO-d_6) δ 12.46 (br s, 1H), 8.26–8.24 (m, 2H), 7.91–7.88 (m, 2H), 7.54 (s, 1H), 7.45–7.44 (m, 1H), 7.18–7.17 (m, 1H); ^{13}C NMR (100 MHz, DMSO-d_6) δ 169.0, 167.4, 154.7, 151.0, 147.0, 134.8, 125.3, 125.1, 122.6, 121.3, 117.9, 113.7; HRMS (ESI): calculated for $C_{14}H_8N_2O_5S$, 315.0076 $[M-H]^-$; found, 315.0081; HPLC analysis 98.83 % (R_t: 13.78 min).

5-((5-(4-nitrophenyl)thiophene-2-yl)methylene)-2-thioxoimidazolidin-4-one (**9a**). Following the *GP2*, **2b** (100 mg, 0.43 mmol) and 2-thiohydantoin (59 mg, 0.51 mmol) were used to afford **9a** (138 mg, 97 %) as

a maroon powder. ^{1}H NMR (400 MHz, DMSO-d_6) δ 12.43 (br s, 1H), 12.06 (br s, 1H), 8.28–8.26 (m, 2H), 7.96–7.93 (m, 2H), 7.89–7.87 (m, 2H), 6,64 (s, 1H); ^{13}C NMR (100 MHz, DMSO-d_6) δ 179.3, 165.9, 146.9, 144.1, 139.7, 138.4, 132.8, 129.1, 127.4, 126.5, 125.1, 103.9; HRMS (ESI): calculated for $C_{14}H_9N_3O_3S_2$, 330.0007 [M−H]$^-$; found, 330.0009; HPLC analysis 98.29 % (R_t: 5.71 min).

5-((5-(4-nitrophenyl)thiophene-2-yl)methylene)imidazolidine-2,4-dione (**9b**). Following the *GP2*, **2b** (90 mg, 0.39 mmol) and hydantoin (46 mg, 0.46 mmol) were used to afford **9b** (42 mg, 35 %) as a maroon powder. ^{1}H NMR (400 MHz, DMSO-d_6) δ 11.34 (br s, 1H), 10.48 (br s, 1H), 8.27–8.25 (m, 2H), 7.93–7.91 (m, 2H), 7.85–7.84 (m, 1H), 7.66–7.65 (m, 1H), 6.59 (s, 1H); ^{13}C NMR (100 MHz, DMSO-d_6) δ 165.5, 155.88, 146.7, 142.5, 140.0, 139.1, 131.2, 128.8, 127.9, 126.4, 125.0, 101.2; HRMS (ESI): calculated for $C_{14}H_9N_3O_4S$, 314.0236 [M−H]$^-$; found, 314.0938; HPLC analysis 99.23 % (R_t: 12.20 min).

5-((5-(4-nitrophenyl)thiophene-2-yl)methylene)-2-thioxothiazolidin-4-one (**9c**). Following the *GP2*, **2b** (49 mg, 0.21 mmol) and rhodanine (33 mg, 0.25 mmol) were used to afford **9c** (62 mg, 84 %) as a maroon powder. ^{1}H NMR (400 MHz, DMSO-d_6) δ 13.81 (Br s, 1H), 8.23–8.21 (m, 2H), 8.00–7.96 (m, 2H), 7.90–7.89 (m, 1H), 7.84 (s, 1H), 7.72–7.71 (m, 1H); ^{13}C NMR (100 MHz, DMSO-d_6) δ 194.7, 169.4, 148.0, 147.3, 139.6,139.0,137.3, 128.9,127.0, 125.0, 124.9, 124.4; HRMS (ESI): calculated for $C_{14}H_8N_2O_4S_2$ 346.9619 [M−H]$^-$; found, 346.9622; HPLC analysis 95.86 % (R_t: 6.50 min).

5-((5-(4-nitrophenyl)thiophene-2-yl)methylene)thiazolidine-2,4-dione (**9d**). Following the *GP2*, **2b** (72 mg, 0.31 mmol) and 2,4-dioxothiazolidine (43 mg, 0.37 mmol) were used to afford 9d (56 mg, 55 %) as a maroon powder. ^{1}H NMR (400 MHz, DMSO-d_6) δ 12.64 (br s, 1H), 8.28–8.25 (m, 2H), 8.04–8.00 (m, 3H), 7.94–7.93 (m, 1H), 7.74–7.73 (m, 1H); ^{13}C NMR (100 MHz, DMSO-d_6) δ 167.4, 167.3, 147.3, 146.9, 146.9, 139.5, 139.2, 136.6, 128.7, 127.0, 125.0, 123.0; HRMS (ESI): calculated for $C_{14}H_8N_2O_4S_2$, 330.9847 [M−H]$^-$; found, 330.9850; HPLC analysis 95.51 % (R_t: 6.27 min).

5-((6-(4-nitrophenyl)pyridin-2-yl)methylene)-2-thioxothiazolidin-4-one (**10a**). Following the *GP2*, **2c** (70 mg, 0.31 mmol) and rhodanine (43 mg, 0.37 mmol) were used to afford **10a** (51 mg, 51 %) as a brown powder. ^{1}H NMR (400 MHz, DMSO-d_6) δ 13.77 (br s, 1H), 8.44–8.38 (m, 4H), 8.15–8.10 (m, 2H), 8.00–7.95 (m, 1H), 7.76 (s, 1H); ^{13}C NMR (100 MHz, DMSO-d_6) δ 201.4, 169.9, 155.1, 151.8, 148.5, 144.3, 139.5, 130.5, 128.7, 128.6, 127.7, 124.6, 122.5; HRMS (ESI): calculated for $C_{15}H_9N_3O_3S_2$ 342.0007 [M−H]$^-$; found, 342.0012; HPLC analysis 99.25 % (R_t: 15.20 min).

5-((6-(4-nitrophenyl)pyridin-2-yl)methylene)thiazolidine-2,4-dione (**10b**). Following the *GP2*, **2c** (70 mg, 0.31 mmol) and 2,4-dioxothiazolidine (43 mg, 0.37 mmol) were used to afford **10b** (51 mg, 51 %) as a brown powder. ^{1}H NMR (400 MHz, DMSO-d_6) δ 12.56 (br s, 1H), 8.45 (s, 4H), 8.18–8.10 (m, 2H), 7.96–7.92 (m, 2H); ^{13}C NMR (100 MHz, DMSO-d_6) δ 174.7, 173.3, 154.4, 153.0, 148.4, 144.5, 139.2, 133.2, 128.5, 127.7, 125.2, 124.6, 121.3; HRMS (ESI): calculated for $C_{15}H_9N_3O_4S$, 326.0236 [M−H]$^-$; found, 326.0242; HPLC analysis 95.45 % (R_t: 13.86 min).

5-((1-(4-nitrophenyl)-1H-pyrazol-3-yl)methylene)-2-thioxothiazolidin-4-one (**11a**). Following the *GP2*, **2d** (85 mg, 0.39 mmol) and rhodanine (63 mg, 0.47 mmol) were used to afford **11a** (103 mg, 79 %) as a yellow powder. ^{1}H NMR (400 MHz, DMSO-d_6) δ 13.66 (br s, 1H), 8.80–8.78 (m, 1H), 8.39–8.37 (m, 2H), 8.12–8.09 (m, 2H), 7.50 (s, 1H), 7.01–7.00 (m, 1H); ^{13}C NMR (100 MHz, DMSO-d_6) δ 199.4, 169.6, 148.9, 145.9, 143.6, 131.5, 128.3, 126.1, 120.8, 119.3, 113.4; HRMS (ESI): calculated for $C_{13}H_8N_4O_3S_2$, 330.9960 [M−H]$^-$; found, 330.9963; HPLC analysis 99.25 % (R_t: 15.20 min).

5-((6-(4-nitrophenyl)pyridin-2-yl)methylene)thiazolidine-2,4-dione (**11b**). Following the *GP2*, **2d** (75 mg, 0.35 mmol) and 2,4-dioxothiazolidine (48 mg, 0.41 mmol) were used to afford **11b** (104 mg, 94 %) as a pale yellow powder. ^{1}H NMR (400 MHz, DMSO-d_6) δ 12.42 (br s, 1H), 8.75–8,74 (m, 1H), 8.34–8.30 (m, 2H), 8.08–8.04 (m, 2H), 7.60 (s, 1H), 6.94–6.94 (m, 1H); ^{13}C NMR (100 MHz, DMSO-d_6) δ 170.4, 167.6, 148.9, 145.7, 143.6, 131.1, 126.5, 126.0, 121.4, 119.1, 112.9; HRMS (ESI): calculated for $C_{13}H_8N_4O_4S$, 315.0188 [M−H]$^-$; found, 315.0194; HPLC analysis 96.72 % (R_t: 12.85 min).

3-(5-((5-(4-nitrophenyl)furan-2-yl)methylene)-2,4-dioxothiazolidin-3-yl)propanoinc acid (**12**). Following the *GP2*, **2a** (93 mg, 0.43 mmol) and **6b** (89 mg, 0.47 mmol) were used to afford **12** (102 mg, 50 %) as a yellow powder. ^{1}H NMR (400 MHz, DMSO-d_6) δ 12.48 (br s, 1H), 8.36–8.34 (m, 2H), 8.02–8.00 (m, 2H), 7.78 (s, 1H), 7.56–7.56 (m, 1H), 7.32–7.31 (m, 1H), 3.87 (t, 2H, J = 7.2 Hz), 2.61 (t, 2H, J = 7.2 Hz); ^{13}C NMR (100 MHz, DMSO-d_6) δ 172.3, 168.1, 165.5, 155.0, 151.0, 147.2, 134.8, 125.4, 125.2, 121.9, 120.1, 118.9, 113.8, 37.8, 32.0; HRMS (ESI): calculated for C17H12N2O7S, 387.0287 [M−H]-; found, 387.0387; HPLC analysis 98.04 % (R_t: 13.30 min).

2-(5-((6-(4-nitrophenyl)pyridin-2-yl)methylene)-2,4-dioxothiazolidin-3-yl)acetic acid (**13a**). Following the *GP2*, **2c** (59 mg, 0.26 mmol) and **6a** (54 mg, 0.31 mmol) were used to afford **13a** (27 mg, 27 %) as an off-white powder. ^{1}H NMR (400 MHz, DMSO-d_6) δ 8.47 (s, 4H), 8.20–8.12 (m, 2H), 8.02 (s, 1H), 7.99–7.97 (m, 1H), 3.87 (s, 2H); ^{13}C NMR (100 MHz, DMSO-d_6) δ 170.8, 166.8, 166.3, 154.7, 152.3, 148.5, 144.4, 139.6, 128.6, 128.5, 128.3, 127.3, 124.7, 122.3, 45.9; HRMS (ESI): calculated for $C_{17}H_{11}N_3O_6S$, 384.0290 [M−H]$^-$; found, 384.0335; HPLC analysis 97.06 % (R_t: 13.19 min).

3-(5-((6-(4-nitrophenyl)pyridin-2-yl)methylene)-2,4-dioxothiazolidin-3-yl)propanoic acid (**13b**). Following the *GP2*, **2c** (53 mg, 0.23 mmol) and **6b** (53 mg, 0.28 mmol) were used to afford **13b** (38 mg, 41 %) as a beige powder. ^{1}H NMR (400 MHz, DMSO-d_6) δ 12.46 (s, 1H), 8.44–8.40 (m, 4H), 8.16–8.09 (m, 2H), 8.01 (s, 1H), 7.96–7.94 (m, 1H), 3.88 (t, 2H, J = 7.2 Hz), 2.62 (t, 2H, J = 7.2 Hz); ^{13}C NMR (100 MHz, DMSO-d_6) δ 172.4, 170.8, 166.0, 154.7, 151.9, 148.5, 144.2, 139.6, 129.2, 128.6, 128.5, 126.3, 124.7, 125.5, 37.4, 32.0; HRMS (ESI): calculated for $C_{18}H_{13}N_3O_6S$, 398.0447 [M−H]$^-$; found, 398.0556; HPLC analysis 98.23 % (R_t: 13.23 min).

4-(5-((6-(4-nitrophenyl)pyridin-2-yl)methylene)-2,4-dioxothiazolidin-3-yl)butanoic acid (**13c**). Following the *GP2*, **2c** (56 mg, 0.25 mmol) and **6c** (60 mg, 0.29 mmol) were used to afford **13c** (68 mg, 67 %) as a beige powder. ^{1}H NMR (400 MHz, DMSO-d_6) δ 12.15 (br s, 1H), 8.45–8.39 (m, 4H), 8.16–8.09 (m, 2H), 8.00 (s, 1H), 7.96–7.94 (m, 1H), 3.71 (t, 2H, J = 6.8 Hz), 2.30 (t, 2H, J = 7.2 Hz), 1.87–1.80 (m, 2H); ^{13}C NMR (100 MHz, DMSO-d_6) δ 174.3, 171.2, 166.4, 154.7, 152.0, 148.5, 144.2, 139.5, 129.0, 128.5, 128.5, 126.4, 124.7, 122.4, 40.9, 31.3, 23.0; HRMS (ESI): calculated for $C_{19}H_{15}N_3O_6S$, 412.0603 [M−H]$^-$; found, 412.0705; HPLC analysis 99.34 % (R_t: 13.61 min).

3-(2-hydroxyethyl)-5-((6-(4-nitrophenyl)pyridin-2-yl)methylene)thiazolidine-2,4-dione (**13d**). Following the *GP2*, **2c** (260 mg, 1.14 mmol) and **4a** (220 mg, 1.37 mmol) were used to afford **13d** (280 mg, 66 %) as a beige powder. ^{1}H NMR (400 MHz, DMSO-d_6) δ 8.45–8.40 (m, 4H), 8.16–8.09 (m, 2H), 8.00 (s, 1H), 7.96–7.94 (m, 1H), 4.94 (t, 1H, J = 6.4 Hz), 3.74 (t, 2H, J = 6.0 Hz), 3.60 (q, 2H, J = 5.6 Hz); ^{13}C NMR (100 MHz, DMSO-d_6) δ 171.0, 163.4, 154.7, 152.0, 148.5, 144.2, 139.5, 128.9, 128.6, 128.4, 126.5, 124.6, 122.4, 57.7, 44.1; HRMS (ESI): calculated for $C_{17}H_{13}N_3O_5S$, 370.0498 [M−H]$^-$; found, 370.0568; HPLC analysis 97.55 % (R_t: 13.19 min).

3-(3-hydroxypropyl)-5-((6-(4-nitrophenyl)pyridin-2-yl)methylene)thiazolidine-2,4-dione (**13e**). Following the *GP2*, **2c** (81 mg, 0.35 mmol) and **4b** (75 mg, 0.43 mmol) were used to afford **13e** (39 mg, 29 %) as a beige powder. ^{1}H NMR (400 MHz, DMSO-d_6) δ 8.44–8.39 (m, 4H), 8.15–8.09 (m, 2H), 8.00 (s, 1H), 7.96–7.94 (m, 1H), 4.56 (t, 1H, J = 5.2 Hz), 3.73 (t, 2H, J = 6.8 Hz), 3.47 (q, 2H, J = 6.0 Hz), 1.78–1.72 (m, 2H); ^{13}C NMR (100 MHz, DMSO-d_6) δ 171.0, 166.3, 154.7, 152.0, 148.5, 144.2, 139.5, 129.0, 128.6, 128.5, 126.4, 124.6, 122.4, 59.0, 30.9; HRMS (ESI): calculated for $C_{18}H_{15}N_3O_5S$, 384.0654 [M−H]$^-$; found, 384.0722; HPLC analysis 99.18 % (R_t: 13.49 min).

3-(2-(dimethylamino)ethyl)-5-((6-(4-nitrophenyl)pyridin-2-yl)methylene)thiazolidine-2,4-dione (**13f**). Following the *GP2*, **2c** (42 mg, 0.18 mmol) and **6d** (41 mg, 0.22 mmol) were used to afford **13f** (41 mg, 57 %) as a beige powder. ^{1}H NMR (400 MHz, DMSO-d_6) δ 8.41–8.36 (m,

4H), 8.14–8.06 (m, 2H), 7.99 (s, 1H), 7.93–7.91 (m, 1H), 3.71 (t, 2H, *J* = 6.4 Hz), 2.46–2.45 (m, 2H), 2.01 (s, 6H); ^{13}C NMR (100 MHz, DMSO-d_6) δ 170.9, 166.2, 154.8, 152.0, 148.6, 144.3, 139.7, 128.3, 128.7, 128.5, 126.3, 124.7, 122.6, 58.2, 45.6, 40.7; HRMS (ESI): calculated for $C_{19}H_{18}N_4O_4S$, 399.1127 [M + H]$^+$; found, 399.1126; HPLC analysis 95.97 % (R_t: 9.51 min).

3-(3-(dimethylamino)propyl)-5-((6-(4-nitrophenyl)pyridin-2-yl)methylene)thiazolidine-2,4-dione (**13 g**). Following the *GP2*, **2c** (68 mg, 0.30 mmol) and **6e** (72 mg, 0.36 mmol) were used to afford **13 g** (44 mg, 36 %) as a beige powder. ^{1}H NMR (400 MHz, DMSO-d_6) δ 8.47–8.42 (m, 4H), 8.19–8.11 (m, 2H), 8.03 (s, 1H), 7.98–7.96 (m, 1H), 3.70 (t, 2H, *J* = 7.2 Hz), 2.25 (t, 2H, *J* = 7.2 Hz), 2.11 (s, 6H), 1.75–1.68 (m, 2H); ^{13}C NMR (100 MHz, DMSO-d_6) δ 171.1, 166.3, 154.8, 152.0, 148.5, 144.3, 139.6, 129.0, 128.6, 128.5, 126.5, 124.7, 122.5, 56.8, 45.5, 25.4; HRMS (ESI): calculated for $C_{20}H_{20}N_4O_4S$, 413.1284 [M + H]$^+$; found, 413.1280; HPLC analysis 99.02 % (R_t: 9.47 min).

3-(2-morpholinoethyl)-5-((6-(4-nitrophenyl)pyridin-2-yl)methylene) thiazolidine-2,4-dione (**13 h**). Following the *GP2*, **2c** (70 mg, 0.31 mmol) and **6f** (84 mg, 0.37 mmol) were used to afford **13 h** (71 mg, 53 %) as a beige powder. ^{1}H NMR (400 MHz, DMSO-d_6) δ 8.46–8.42 (m, 4H), 8.18–8.11 (m, 2H), 8.05 (s, 1H), 7.98–7.97 (m, 1H), 3.80 (t, 2H, *J* = 6.4 Hz), 3.51 (m, 4H), 2.55 (t, 2H, *J* = 6.4 Hz), 2.42 (s, 4H); ^{13}C NMR (100 MHz, DMSO-d6) δ 170.9, 166.2, 154.8, 152.0, 148.5, 144.2, 139.6, 129.3, 128.6, 128.5, 126.2, 124.7, 122.6, 66.7, 55.2, 53.6, 38.6; HRMS (ESI): calculated for $C_{21}H_{20}N_4O_5S$, 441.1233 [M + H]$^+$; found, 441.1290; HPLC analysis 98.74 % (R_t: 9.02 min).

3-(3-morpholinopropyl)-5-((6-(4-nitrophenyl)pyridin-2-yl)methylene) thiazolidine-2,4-dione (**13i**). Following the *GP2*, **2c** (61 mg, 0.27 mmol) and **6 g** (79 mg, 0.32 mmol) were used to afford **13i** (73 mg, 60 %) as a white powder. ^{1}H NMR (400 MHz, DMSO-d_6) δ 8.43 (br s, 4H), 8.17–8.10 (m, 2H), 8.02 (s, 1H), 8.00–7.95 (m, 1H), 3.74 (t, 2H, *J* = 6.8 Hz), 3.51–3.49 (m, 4H), 2.33 (t, 2H, *J* = 6.4 Hz), 2.28 (s, 4H), 1.79–1.73 (m, 2H); ^{13}C NMR (100 MHz, DMSO-d_6) δ 171.1, 166.4, 154.8, 152.0, 148.5, 144.2, 139.6, 129.0, 128.6, 128.5, 126.6, 124.7, 122.5, 66.6, 56.4, 53.8, 40.3, 23.7; HRMS (ESI): calculated for $C_{22}H_{22}N_4O_5S$, 455.1389 [M + H]$^+$; found, 455.1542; HPLC analysis 99.77 % (R_t: 9.02 min).

3-(2-(4-methylpiperazin-1-yl)ethyl)-5-((6-(4-nitrophenyl)pyridin-2-yl) methylene)thiazolidine-2,4-dione (**13j**). Following the *GP2*, **2c** (35 mg, 0.15 mmol) and **6 h** (45 mg, 0.18 mmol) were used to afford **13j** (27 mg, 39 %) as a beige powder. ^{1}H NMR (400 MHz, DMSO-d_6) δ 8.48–8.43 (m, 4H), 8.20–8.13 (m, 2H), 8.06 (s, 1H), 8.00–7.98 (m, 1H), 3.79 (t, 2H, *J* = 6.4 Hz), 2.54 (t, 2H, *J* = 6.4 Hz), 2.42–2.24 (m, 8H), 2.11 (s, 3H); ^{13}C NMR (100 MHz, DMSO-d_6) δ 170.9, 166.2, 154.9, 152.0, 148.6, 144.3, 139.7, 129.2, 128.7, 128.6, 126.3, 124.7, 122.6, 55.2, 54.7, 53.0, 46.1, 38.9; HRMS (ESI): calculated for $C_{22}H_{23}N_5O_4S$, 454.1549 [M + H]$^+$; found, 454.1907; HPLC analysis 98.86 % (R_t: 9.02 min).

3-(2-(4-methylpiperazin-1-yl)ethyl)-5-((6-(4-nitrophenyl)pyridin-2-yl) methylene)thiazolidine-2,4-dione (**13 k**). Following the *GP2*, **2c** (90 mg, 0.39 mmol) and **6i** (122 mg, 0.47 mmol) were used to afford **13 k** (56 mg, 30 %) as a beige powder. ^{1}H NMR (400 MHz, DMSO-d_6) δ 8.45–8.43 (m, 4H), 8.16–8.09 (m, 2H), 8.03–8.02 (m, 1H), 7.96–7.95 (m, 1H), 3.72 (t, 2H, *J* = 6.8 Hz), 2.33–2.28 (m, 9H), 2.03–1.94 (m, 4H), 1.77–1.71 (m, 2H; ^{13}C NMR (100 MHz, DMSO-d_6) δ 171.1, 166.4, 154.7, 152.0, 148.5, 144.2, 139.6, 128.9, 128.6, 128.4, 126.6, 124.7, 122.4, 55.9, 55.0, 53.0, 46.0, 24.0; HRMS (ESI): calculated for $C_{23}H_{25}N_5O_4S$, 468.1706 [M + H]$^+$; found, 468.1705; HPLC analysis 99.37 % (R_t: 9.54 min).

5-((6-(4-nitrophenyl)pyridin-2-yl)methylene)-3-(2-(piperidin-1-yl) ethyl)thiazolidine-2,4-dione (**13 l**). Following the *GP2*, **2c** (68 mg, 0.30 mmol) and **6j** (81 mg, 0.36 mmol) were used to afford **13 l** (62 mg, 48 %) as a light yellow powder. ^{1}H NMR (400 MHz, DMSO-d_6) δ 8.48–8.43 (m, 4H), 8.20–8.12 (m, 2H), 8.06 (s, 1H), 8.00–7.98 (m, 1H), 3.78 (t, 2H, *J* = 6.4 Hz), 2.45 (s, 2H), 2.37 (br s, 4H), 1.43–1.34 (m, 6H); ^{13}C NMR (100 MHz, DMSO-d_6) δ 170.8, 166.2, 154.8, 152.0, 148.6, 144.3, 139.6, 129.2, 128.7, 128.5, 126.3, 124.7, 122.6, 55.4, 54.4, 39.0, 26.1, 24.4; HRMS (ESI): calculated for $C_{22}H_{22}N_4O_4S$, 439.1440 [M + H]+; found, 439.1523; HPLC analysis 96.10 % (R_t: 9.43 min).

5-((6-(4-nitrophenyl)pyridin-2-yl)methylene)-3-(2-(piperazin-1-yl) ethyl)thiazolidine-2,4-dione (**13q**). Following the *GP2,* **1c** (76 mg, 0.33 mmol) and **6 k** (133 mg, 0.40 mmol) were used to afford **13 m** as a reaction intermediate. The obtained intermediate was suspended in HCl (4 N in 1,4-dioxane) and stirred at RT for 16 h then poured to diethyl ether (Et_2O). The formed precipitate was filtered and washed with Et_2O to collect the title compound **13q** as a light yellow powder (57 mg, 39 % over 2 steps). ^{1}H NMR (400 MHz, DMSO-d_6) δ 8.46–8.41 (m, 4H), 8.18–8.11 (m, 2H), 8.03 (s, 1H), 7.98–7.96 (m, 1H), 3,78 (t, 2H, *J* = 6.4 Hz), 2.64–2.62 (m, 4H), 2.49 (s, 2H), 2.34 (br s, 4H); ^{13}C NMR (100 MHz, DMSO-d_6) δ 170.9, 166.2, 154.8, 152.0, 148.5, 144.2, 139.6, 129.2, 128.6, 128.5, 126.2, 124.7, 122.5, 55.4, 54.4, 46.0, 38.7; HRMS (ESI): calculated for $C_{21}H_{21}N_5O_4S$, 440.1392 [M + H]$^+$; found, 440.1935; HPLC analysis 96.99 % (R_t: 9.04 min).

5-((6-(4-nitrophenyl)pyridin-2-yl)methylene)-3-(3-(piperazin-1-yl)propyl)thiazolidine-2,4-dione dihydrochloride (**13r**). Following the *GP2* and the preparation method of **13q**, **2c** (63 mg, 0.28 mmol) and **6 l** (114 mg, 0.33 mmol) to produce **13n** as a reaction intermediate and **13r** (100 mg, 69 % over 2 steps) as a light brown powder. ^{1}H NMR (400 MHz, DMSO-d_6) δ 12.07 (br s, 1H), 10.12–9.99 (m, 2H), 8.45–8.41 (m, 4H), 8.17–8.11 (m, 2H), 8.03 (s, 1H), 7.99–7.97 (m, 1H), 3.76 (t, 2H, *J* = 6.4 Hz), 3.68–3.66 (m, 2H), 3.57–3.36 (m, 6H), 3.26–3.22 (m, 2H), 2,13–2.09 (m, 2H); ^{13}C NMR (100 MHz, DMSO-d_6) δ 171.3, 166.4, 154.7, 152.0, 148.5, 144.2, 139.6, 129.1, 128.6, 128.5, 126.6, 124.7, 122.5, 53.6, 48.0, 38.7, 22.4; HRMS (ESI): calculated for $C_{22}H_{23}N_5O_4S$, 454.1549 [M + H]$^+$; found, 454.2068; HPLC analysis 98.38 % (R_t: 8.33 min).

3-(2-(cyclohexylamino)ethyl)-5-((6-(4-nitrophenyl)pyridin-2-yl)methylene)thiazolidine-2,4-dione (**13 s**). Following the *GP2* and the preparation method of **13q**, **2c** (102 mg, 0.45 mmol) and **6p** (185 mg, 0.54 mmol) to produce **13p** as a reaction intermediate and **13 s** (100 mg, 64 % over 2 steps) as a beige powder. ^{1}H NMR (400 MHz, DMSO-d_6) δ 8.81–8.80 (m, 2H), 8.42–8.37 (m, 4H), 8.15–8.07 (m, 2H), 8.02 (s, 1H), 7.95–7.93 (m, 1H), 3.94 (t, 2H, *J* = 6.0 Hz), 3.17–3.14 (m, 2H), 3.01 (br s, 1H), 1.95–1.92 (m, 2H), 1.72–1.69 (m, 2H), 1.56–1.53 (m, 1H), 1.28–1.12 (m, 4H), 1.04–0.99 (m, 1H); ^{13}C NMR (100 MHz, DMSO-d_6) δ 171.5, 166.6, 154.9, 152.0, 148.6, 144.2, 139.7, 129.2, 128.6, 128.5, 126.7, 124.8, 122.7, 56.2, 41.3, 37.8, 28.8, 25.2, 24.4; HRMS (ESI): calculated for $C_{23}H_{24}N_4O_4S$, 453.1597 [M + H]$^+$; 453.1594; HPLC analysis 98.46 % (R_t: 10.59 min).

3-(3-(cyclohexylamino)propyl)-5-((6-(4-nitrophenyl)pyridin-2-yl) methylene)thiazolidine-2,4-dione hydrochloride (**13 t**). Following the *GP2* and the preparation method of **13q**, **2c** (201 mg, 0.88 mmol) and **6p** (377 mg, 1.06 mmol) to produce **13p** as a reaction intermediate and **13u** (58 mg, 20 % over 2 steps) as a beige powder. ^{1}H NMR (400 MHz, DMSO-d_6) δ 9.03 (br s, 2H), 8.42 (br s, 4H), 8.17–8.10 (m, 2H), 8.03 (s, 1H), 7.98–7.97 (m, 1H), 3.76 (t, 2H, *J* = 6.4 Hz), 2.95 (br s, 3H), 2.04–2.02 (m, 4H), 1.77–1.74 (m, 2H), 1.61–1.58 (m, 1H), 1.39–1.05 (m, 5H); ^{13}C NMR (100 MHz, DMSO-d6) δ 171.3, 166.4, 154.7, 151.9, 148.5, 144.2, 139.6, 129.2, 128.6, 128.5, 126.4, 124.6, 122.5, 56.4, 41.7, 39.0, 28.9, 25.2, 24.9, 24.4; HRMS (ESI): calculated for $C_{24}H_{26}N_4O_4S$, 467.1753 [M + H]$^+$; found, 467.2217; HPLC analysis 99.19 % (R_t: 10.00 min).

3-(4-(4-methylpiperazin-1-yl)-4-oxobutyl)-5-((6-(4-nitrophenyl)pyridin-2-yl)methylene)thiazolidine-2,4-dione (**14a**). To a solution of **13c** (64 mg, 0.15 mmol) in CH_2Cl_2, 1-methylpiperazine (26 μL, (0.23 mmol), 1-(3-dimethylaminopropyl)-3-ethylcarbodiimide hydrochloride (36 mg, 0.19 mmol), and 4-dimethylaminopyridine (23 mg, 0.19 mmol), and $(iPr)_2EtN$ (54 μL, 0.31 mmol) were added. The mixture was then stirred at RT for 16 h. After the reaction completion, the reaction solution was condensed *in vacuo,* and the crude was purified by column chromatography (2 % MeOH / CH_2Cl_2) to afford the title compound **14a** (45 mg, 59 %) as an off-white powder. ^{1}H NMR (400 MHz, DMSO-d_6) δ 8.40–8.35 (m, 4H), 8.12–8.04 (m, 2H), 7.96 (s, 1H), 7.92–7.90 (m, 1H), 3,63 (t, 2H, *J* = 6.8 Hz), 3.35 (br s, 4H), 2.33–2.26 (m, 6H), 2,18 (s, 3H),

1.81–1.75 (m, 2H); ^{13}C NMR (100 MHz, DMSO-d_6) δ 171.2, 170.2, 166.4, 154.8, 152.1, 148.5, 144.3, 139.6, 128.9, 128.6, 128.5, 126.6, 124.7, 122.5, 54.8, 54.5, 44.7, 41.3, 29.8, 23.1; HRMS (ESI): calculated for $C_{24}H_{25}N_5O_5S$, 496.1655 $[M + H]^+$; found, 496.1653; HPLC analysis 99.33 % (R_t: 9.52 min).

3-(4-morpholino-4-oxobutyl)-5-((6-(4-nitrophenyl)pyridin-2-yl)methylene)thiazolidine-2,4-dione (**14b**). Following the procedure of **14a**, **13c** (42 mg, 0.10 mmol) and morpholine (10 μL, 0.12 mmol) were used to afford **14b** (40 mg, 82 %) as a white powder. ^{1}H NMR (400 MHz, DMSO-d_6) δ 8.48–8.43 (m, 4H), 8.20–8.12 (m, 2H), 8.05 (s, 1H), 8.00–7.99 (m, 1H), 3.71 (t, 2H, J = 6.8 Hz), 3.57–3.51 (m, 4H), 3.41–3.40 (m, 4H), 2.38 (t, 2H, J = 7.2 Hz), 1.89–1.82 (m, 2H); ^{13}C NMR (100 MHz, DMSO-d_6) δ 171.2, 170.4, 166.4, 154.8, 152.1, 148.6, 144.3, 139.7, 128.9, 128.6, 128.5, 126.7, 124.7, 122.5, 66.5, 52.7, 45.7, 42.0, 41.3, 29.7, 23.1; HRMS (ESI): calculated for $C_{23}H_{22}N_4O_6S$, 483.1338 $[M + H]^+$; found, 483.1355; HPLC analysis 98.43 % (R_t: 13.77 min).

5-((6-(4-nitrophenyl)pyridin-2-yl)methylene)-3-(4-oxo-4-(piperazin-1-yl)butyl)thiazolidine-2,4-dione hydrochloride (**14d**). Following the preparation method of **14a** and **13q**, **13c** (73 mg, 0.18 mmol) and 1-Bocpiperazine (39 mg, 0.21 mmol) to produce **14c** as a reaction intermediate and **14d** (27 mg, 29 % over 2 steps) as an off-white powder. ^{1}H NMR (400 MHz, DMSO-d_6) δ 9.41 (br s, 2H), 8.47–8.42 (m, 4H), 8.19–8.11 (m, 2H), 8.05 (s, 1H), 8.02–8.00 (m, 1H), 3.73–3.66 (m, 6H), 3.09–3.02 (m, 4H), 2.43 (t, 2H, J = 6.8 Hz), 1.90–1.83 (m, 2H); ^{13}C NMR (100 MHz, DMSO-d_6) δ 171.3, 170.5, 166.5, 154.8, 152.1, 148.5, 144.2, 139.6, 129.0, 128.6, 128.5, 126.6, 124.7, 122.5, 43.0, 42.2, 41.2, 38.4, 29.4, 23.0; HRMS (ESI): calculated for $C_{23}H_{23}N_5O_5S$, 482.1498 $[M + H]^+$; found, 482.1625; HPLC analysis 99.35 % (R_t: 8.95 min).

4.2. Topflash reporter gene assay

TOPflash reporter gene-incorporated HEK293 cells were seeded at 15,000 cells/well in 24-well plates (Greiner Bio-One) for 18 h. l-CM (L-cell-conditioned media) or Wnt3a-CM (Wnt3a conditioned media) with DMSO or the compounds was added to the wells at a concentration of 1 μM for 18 h. After treatment, the cells were harvested and lysed with 60 μL of reporter lysis buffer (Promega E387A), according to the manufacturer's instructions. The lysates were centrifuged (4 °C, 12,000 RPM, 10 min), and 20 μL of the supernatant was collected to measure luciferase activity. Relative fluorescence activity was normalized to the value of Wnt3a-CM, with DMSO as a control.

4.3. Immunoblotting analysis

SW480 cells were seeded at 20,000 cells/well in 6-well plates. After 18 h, the cells were treated with DMSO or the compounds at 5 and 25 μM for 24 h. The cells were then lysed using a radioimmunoprecipitation assay buffer (Millipore). Proteins were separated on a 6–15 % sodium dodecyl sulfate–polyacrylamide gel and transferred to a nitrocellulose membrane (Whatman). Immunoblotting was performed using the following primary antibodies: anti-pan-Ras monoclonal (clone Ras10, Millipore, MABS195; 1:3,000), anti-β-catenin (Santa Cruz Biotechnology; sc-7199; 1:3,000), and anti-α-tubulin (Cell Signaling Technology, #3873S; 1:10,000) for 1.5 h at room temperature, followed by horseradish peroxidase-conjugated secondary antibodies: anti-mouse (Cell Signaling Technology, #7076, 1:3,000) or anti-rabbit (Bio-Rad, #1706515; 1:3,000) for 1 h at room temperature. The bands were detected by enhanced chemiluminescence (Amersham Biosciences) using a luminescent image analyzer (LAS-3000, Fuji Film).

4.4. Colony formation assay

SW480 cells were seeded in 12-well plates at a density of 500 cells/well. The cells were then treated with DMSO, **1**, **13d** or **13e** at 5 and 25 μM for every 72 h until visible colonies were formed. For counting colony number, cells were fixed in 4 % paraformaldehyde for 30 min and stained with 0.5 % crystal violet in 20 % EtOH for 30 min.

4.5. Fluorescence spectroscopy

The dissociation constants (K_d) for the binding of **KYA1797K** and **13d** to Axin74-220 were determined through protein fluorescence intensity using a spectrofluorophotometer (RF-5301PC, Shimadzu). Experiments were performed in 25 mM Na_3PO_4, 300 mM NaCl and 20 mM β-mercaptoethanol. The compounds were titrated with Axin74-220 up to the ratio indicated in the legend of each figure in the thermostat cuvette. K_d values of the compounds were calculated using the following equation: $\log((F0 - F)/F) = \log(1/K_d) + n \log[\text{ligand}]$, where F0 and F denote the fluorescence intensity of Axin74-220 at 360 nm wavelength in the absence and presence of the compounds, respectively.

4.6. Docking study

All molecular docking analyses were performed using Discovery Studio 2022 (Biovia), using the CHARM force field. The structure of the RGS homologous domain of axin (1DK8) was obtained from the protein databank and refined by removing the water molecules and adding hydrogen atoms to the entire protein. Ligandfit and CDOCKER docking analyses were performed for ligand docking. The previously reported crystal structure of axin was used to determine the binding sites [34] of the designed compounds. Ten poses were generated for each docking compound to derive the binding energy of the most probable prospective binding mode.

4.7. Solubility evaluation

1.5 mg powder of evaluated analogs were suspended in 1.5 mL of PBS or diluted water. Each suspension was sonicated for 15 min and shaken for 30 min at 37 °C, then filtered through a hydrophilic GHB membrane (pore size = 0.2 μm). The concentration of the filtered solution was calculated through concentration-UV absorbance curves. For generation of concentration-UV absorbance curve, each compound was completely dissolved in DMSO at a concentration of 500 μg/mL. The solution was serially diluted (500, 166.67, 55.56, 18.52, 6.17, 2.06, 0.69, 0.23 μg/mL), to collect aliquot of each sample. HPLC analysis was performed to obtain the UV absorbance peak area of the aliquots (Information of HPLC system is described in 4.1.).

Declaration of Competing Interest

The authors declare that they have no known competing financial interests or personal relationships that could have appeared to influence the work reported in this paper.

Data availability

Data will be made available on request.

Acknowledgements

This research was supported by a grant from Translational Research Center for Protein Function Control (TRCP) funded by the Ministry of Science, ICT and Future Planning (MSIP) of Korea [NRF-2009-0083522 and NRF-2016R1A5A1004694], the Korea Health Technology R&D Project through the Korea Health Industry Development Institute (KHIDI), funded by the Ministry of Health & Welfare, Republic of Korea [HI14C1324], Ministry of Science and ICT [NRF-2019M3E5D5066690] and Bio & Medical Technology Development Program of the National Research Foundation (NRF)& funded by the Korean government (MSIP&MOHW) [2016M3A9B5941215].

Appendix A. Supplementary material

Supplementary data to this article can be found online at https://doi.org/10.1016/j.bioorg.2022.106234.

References

[1] H. Sung, J. Ferlay, R.L. Siegel, M. Laversanne, I. Soerjomataram, A. Jemal, F. Bray, Global Cancer Statistics 2020: GLOBOCAN Estimates of Incidence and Mortality Worldwide for 36 Cancers in 185 Countries, CA A Cancer J Clin 71 (3) (2021) 209–249.

[2] G.A. Hobbs, C.J. Der, K.L. Rossman, RAS isoforms and mutations in cancer at a glance, J. Cell Sci. 129 (7) (2016) 1287–1292, https://doi.org/10.1242/jcs.182873.

[3] S.K. Lee, J.H. Hwang, K.Y. Choi, Interaction of the Wnt/β-catenin and RAS-ERK pathways involving co-stabilization of both β-catenin and RAS plays important roles in the colorectal tumorigenesis, Adv. Biol. Regul. 68 (2018) 46–54, https://doi.org/10.1038/s41698-018-0049-y.

[4] R. Fodde, The APC gene in colorectal cancer, Eur. J. Cancer 38 (7) (2002) 867–871, https://doi.org/10.1016/S0959-8049(02)00040-0.

[5] M.S. Boguski, F. McCormick, Proteins regulating Ras and its relatives, Nature 366 (6456) (1993) 643–654, https://doi.org/10.1038/366643a0.

[6] P. Chardin, J. Camonis, N. Gale, L. van Aelst, J. Schlessinger, M. Wigler, D. Bar-Sagi, Human Sos1: a guanine nucleotide exchange factor for Ras that binds to GRB2, Science 260 (5112) (1993) 1338–1343, https://doi.org/10.1126/science.8493579.

[7] C.J. Marshall, Ras Effectors, Curr. Opin. Cell Biol. 8 (2) (1996) 197–204, https://doi.org/10.1016/S0955-0674(96)80066-4.

[8] M. Milburn, L. Tong, A. deVos, A. Brunger, Z. Yamaizumi, S. Nishimura, S. Kim, Molecular Switch for Signal Transduction: Structural Differences Between Active and Inactive Forms of Protooncogenic Ras Proteins, Science 247(4945) (1990) 939–945, https://doi.org/10.1126/science.2406906.

[9] J.L. Bos, H. Rehmann, A. Wittinghofer, GEFs and GAPs: Critical Elements in the Control of Small G Proteins, Cell 129 (5) (2007) 865–877, https://doi.org/10.1016/j.cell.2007.05.018.

[10] S.M. Margarit, H. Sondermann, B.E. Hall, B. Nagar, A. Hoelz, M. Pirruccello, D. Bar-Sagi, J. Kuriyan, Structural Evidence for Feedback Activation by Ras·GTP of the Ras-Specific Nucleotide Exchange Factor SOS, Cell 112 (5) (2003) 685–695, https://doi.org/10.1016/s0092-8674(03)00149-1.

[11] C. Kötting, M. Blessenohl, Y. Suveyzdis, R.S. Goody, A. Wittinghofer, K. Gerwert, A phosphoryl transfer intermediate in the GTPase reaction of Ras in complex with its GTPase-activating protein, Proc. Natl. Acad. Sci. U. S. A. 103 (38) (2006) 13911–13916, https://doi.org/10.1073/pnas.0604128103.

[12] Y. Pylayeva-Gupta, E. Grabocka, D. Bar-Sagi, RAS oncogenes: weaving a tumorigenic web, Nat. Rev. Cancer 11 (11) (2011) 761–774, https://doi.org/10.1038/nrc3106.

[13] A.D. Cox, S.W. Fesik, A.C. Kimmelman, J. Luo, C.J. Der, Drugging the undruggable RAS: Mission possible? Nat. Rev. Drug Discov. 13 (11) (2014) 828–851, https://doi.org/10.1038/nrd4389.

[14] L.P. Wright, M.R. Philips, Thematic review series: Lipid Posttranslational Modifications CAAX modification and membrane targeting of Ras, J. Lipid Res. 47 (5) (2006) 883–891, https://doi.org/10.1194/jlr.R600004-JLR200.

[15] J. Zujewski, I.D. Horak, C.J. Bol, R. Woestenborghs, C. Bowden, D.W. End, V.K. Piotrovsky, J. Chiao, R.T. Belly, A. Todd, W.C. Kopp, D.R. Kohler, C. Chow, M. Noone, F.T. Hakim, G. Larkin, R.E. Gress, R.B. Nussenblatt, A.B. Kremer, K.H. Cowan, Phase I and Pharmacokinetic Study of Farnesyl Protein Transferase Inhibitor R115777 in Advanced Cancer, J. Clin. Oncol. 18(4) (2000) 927-927. 10.1200/JCO.2000.18.4.927.

[16] M. Liu, M.S. Bryant, J. Chen, S. Lee, B. Yaremko, P. Lipari, M. Malkowski, E. Ferrari, L. Nielsen, N. Prioli, J. Dell, D. Sinha, J. Syed, W.A. Korfmacher, A. A. Nomeir, C.C. Lin, L. Wang, A.G. Taveras, R.J. Doll, F.G. Njoroge, A.K. Mallams, S. Remiszewski, J.J. Catino, V.M. Girijavallabhan, P. Kirschmeier, W.R. Bishop, Antitumor Activity of SCH 66336, an Orally Bioavailable Tricyclic Inhibitor of Farnesyl Protein Transferase, Human Tumor Xenograft Models and Wap-ras Transgenic Mice, Cancer Res. 58 (21) (1998) 4947–4956.

[17] E.L.H. Leung, L.X. Luo, Z.Q. Liu, V.K.W. Wong, L.L. Lu, Y. Xie, N. Zhang, Y.Q. Qu, X.X. Fan, Y. Li, M. Huang, D.K. Xiao, J. Huang, Y.L. Zhou, J.X. He, J. Ding, X.J. Yao, D.C. Ward, L. Liu, Inhibition of KRAS-dependent lung cancer cell growth by deltarasin: blockage of autophagy increases its cytotoxicity, Cell Death Dis. 9 (2) (2018) 216, https://doi.org/10.1038/s41419-017-0065-9.

[18] B. Papke, S. Murarka, H.A. Vogel, P. Martín-Gago, M. Kovacevic, D.C. Truxius, E. K. Fansa, S. Ismail, G. Zimmermann, K. Heinelt, C. Schultz-Fademrecht, A. Al Saabi, M. Baumann, P. Nussbaumer, A. Wittinghofer, H. Waldmann, P.I. H. Bastiaens, Identification of pyrazolopyridazinones as PDEδ inhibitors, Nat. Commun. 7 (1) (2016) 11360, https://doi.org/10.1038/ncomms11360.

[19] D. Kessler, M. Gmachl, A. Mantoulidis, L.J. Martin, A. Zoephel, M. Mayer, A. Gollner, D. Covini, S. Fischer, T. Gerstberger, T. Gmaschitz, C. Goodwin, P. Greb, D. Häring, W. Hela, J. Hoffmann, J. Karolyi-Oezguer, P. Knesl, S. Kornigg, M. Koegl, R. Kousek, L. Lamarre, F. Moser, S. Munico-Martinez, C. Peinsipp, J. Phan, J. Rinnenthal, J. Sai, C. Salamon, Y. Scherbantin, K. Schipany, R. Schnitzer, A. Schrenk, B. Sharps, G. Siszler, Q. Sun, A. Waterson, B. Wolkerstorfer, M. Zeeb, M. Pearson, S.W. Fesik, D.B. McConnell, Drugging an undruggable pocket on KRAS, Proc. Natl. Acad. Sci. U. S. A. 116 (32) (2019) 15823–15829, https://doi.org/10.1073/pnas.1904529116.

[20] T. Maurer, L.S. Garrenton, A. Oh, K. Pitts, D.J. Anderson, N.J. Skelton, B.P. Fauber, B. Pan, S. Malek, D. Stokoe, M.J.C. Ludlam, K.K. Bowman, J. Wu, A.M. Giannetti, M.A. Starovasnik, I. Mellman, P.K. Jackson, J. Rudolph, W. Wang, G. Fang, Small-molecule ligands bind to a distinct pocket in Ras and inhibit SOS-mediated nucleotide exchange activity, Proc. Natl. Acad. Sci. U. S. A. 109 (14) (2012) 5299–5304, https://doi.org/10.1073/pnas.1116510109.

[21] J.O. Agola, L. Hong, Z. Surviladze, O. Ursu, A. Waller, J.J. Strouse, D.S. Simpson, C. E. Schroeder, T.I. Oprea, J.E. Golden, J. Aubé, T. Buranda, L.A. Sklar, A. Wandinger-Ness, A Competitive Nucleotide Binding Inhibitor: In Vitro Characterization of Rab7 GTPase Inhibition, ACS Chem. Biol. 7(6) (2012) 1095-1108. 10.1021/cb3001099.

[22] I.M. Karaguni, P. Herter, P. Debruyne, S. Chtarbova, A. Kasprzynski, U. Herbrand, M.R. Ahmadian, K.H. Glüsenkamp, G. Winde, M. Mareel, T. Möröy, O. Müller, The New Sulindac Derivative IND 12 Reverses Ras-induced Cell Transformation, Cancer Res. 62 (6) (2002) 1718–1723.

[23] F. Shima, Y. Yoshikawa, M. Ye, M. Araki, S. Matsumoto, J. Liao, L. Hu, T. Sugimoto, Y. Ijiri, A. Takeda, Y. Nishiyama, C. Sato, S. Muraoka, A. Tamura, T. Osoda, K. I. Tsuda, T. Miyakawa, H. Fukunishi, J. Shimada, T. Kumasaka, M. Yamamoto, T. Kataoka, In silico discovery of small-molecule Ras inhibitors that display antitumor activity by blocking the Ras-effector interaction, Proc. Natl. Acad. Sci. U. S. A. 110 (20) (2013) 8182–8187, https://doi.org/10.1073/pnas.1217730110.

[24] H.A. Blair, Sotorasib: First Approval, Drugs 81(13) (2021) 1573-1579. 0.1007/s40265-021-01574-2.

[25] J. Canon, K. Rex, A.Y. Saiki, C. Mohr, K. Cooke, D. Bagal, K. Gaida, T. Holt, C.G. Knutson, N. Koppada, B.A. Lanman, J. Werner, A.S. Rapaport, T. San Miguel, R. Ortiz, T. Osgood, J.R. Sun, X. Zhu, J.D. McCarter, L.P. Volak, B.E. Houk, M.G. Fakih, B.H. O'Neil, T.J. Price, G.S. Falchook, J. Desai, J. Kuo, R. Govindan, D.S. Hong, W. Ouyang, H. Henary, T. Arvedson, V.J. Cee, J.R. Lipford, The clinical KRAS(G12C) inhibitor AMG 510 drives anti-tumour immunity, Nature 575(7781) (2019) 217-223. 10.1038/s41586-019-1694-1.

[26] M. Békés, D.R. Langley, C.M. Crews, PROTAC targeted protein degraders: the past is prologue, Nat. Rev. Drug Discov. 21 (3) (2022) 181–200, https://doi.org/10.1038/s41573-021-00371-6.

[27] M.J. Bond, L. Chu, D.A. Nalawansha, K. Li, C.M. Crews, Targeted Degradation of Oncogenic $KRAS^{G12C}$ by VHL-Recruiting PROTACs, ACS Cent. Sci. 6 (8) (2020) 1367–1375, https://doi.org/10.1021/acscentsci.0c00411.

[28] G.M. D'Abaco, R.H. Whitehead, A.W. Burgess, Synergy between Apc min and an activated ras mutation is sufficient to induce colon carcinomas, Mol. Cell. Biol. 16 (3) (1996) 884–891, https://doi.org/10.1128/MCB.16.3.884.

[29] J.M. Bugter, N. Fenderico, M.M. Maurice, Mutations and mechanisms of WNT pathway tumour suppressors in cancer, Nat. Rev. Cancer 21 (1) (2021) 5–21, https://doi.org/10.1038/s41568-020-00307-z.

[30] C. Liu, Y. Li, M. Semenov, C. Han, G.H. Baeg, Y. Tan, Z. Zhang, X. Lin, X. He, Control of β-catenin phosphorylation/degradation by a dual-kinase mechanism, Cell 108 (6) (2002) 837–847, https://doi.org/10.1016/s0092-8674(02)00685-2.

[31] H. Aberle, A. Bauer, J. Stappert, A. Kispert, R. Kemler, beta-catenin is a target for the ubiquitin-proteasome pathway, Embo J. 16 (13) (1997) 3797–3804, https://doi.org/10.1093/emboj/16.13.3797.

[32] W.J. Jeong, E.J. Ro, K.Y. Choi, Interaction between Wnt/β-catenin and RAS-ERK pathways and an anti-cancer strategy via degradations of β-catenin and RAS by targeting the Wnt/β-catenin pathway, NPJ Precis. Oncol. 2 (1) (2018) 5, https://doi.org/10.1038/s41698-018-0049-y.

[33] S.K. Lee, W.J. Jeong, Y.H. Cho, P.H. Cha, J.S. Yoon, E.J. Ro, S. Choi, J.M. Oh, Y. Heo, H. Kim, D.S. Min, G. Han, W. Lee, K.Y. Choi, β-Catenin-RAS interaction serves as a molecular switch for RAS degradation via GSK3β, EMBO Rep. 19(12) (2018) e46060. 10.15252/embr.201846060.

[34] P.H. Cha, Y.H. Cho, S.K. Lee, J. Lee, W.J. Jeong, B.S. Moon, J.H. Yun, J.S. Yang, S. Choi, J. Yoon, H.Y. Kim, M.Y. Kim, S. Kaduwal, W. Lee, S. Min do, H. Kim, G. Han, K.Y. Choi, Small-molecule binding of the axin RGS domain promotes beta-catenin and Ras degradation, Nat. Chem. Biol. 12(8) (2016) 593-600. 10.1038/nchembio.2103.

[35] K. Ewan, B. Pająk, M. Stubbs, H. Todd, O. Barbeau, C. Quevedo, H. Botfield, R. Young, R. Ruddle, L. Samuel, A. Battersby, F. Raynaud, N. Allen, S. Wilson, B. Latinkic, P. Workman, E. McDonald, J. Blagg, W. Aherne, T. Dale, A Useful Approach to Identify Novel Small-Molecule Inhibitors of Wnt-Dependent Transcription, Cancer Res. 70 (14) (2010) 5963–5973, https://doi.org/10.1158/0008-5472.CAN-10-1028.

[36] B.S. Moon, W.J. Jeong, J. Park, T.I. Kim, S. Min do, K.Y. Choi, Role of oncogenic K-Ras in cancer stem cell activation by aberrant Wnt/β-catenin signaling, J. Natl. Cancer Inst. 106(2) (2014) djt373. 10.1093/jnci/djt373.

[37] B. Beck, C. Blanpain, Unravelling cancer stem cell potential, Nat. Rev. Cancer 13 (10) (2013) 727–738, https://doi.org/10.1038/nrc3597.